

1 **SHORT TITLE**

2

3 *cis*-cinnamic acid is an auxin efflux inhibitor

4

5 **CORRESPONDING AUTHORS**

6

7 Bartel Vanholme

8 Department of Plant Systems Biology, VIB, B-9052 Gent, Belgium

9 Department of Plant Biotechnology and Bioinformatics, Ghent University, B-9052 Gent,
10 Belgium

11 E-mail: bartel.vanholme@psb.vib-ugent.be

12 Telephone: + 32 (0)9 33 13 840

13

14 Wout Boerjan;

15 Department of Plant Systems Biology, VIB, B-9052 Gent, Belgium

16 Department of Plant Biotechnology and Bioinformatics, Ghent University, B-9052 Gent,
17 Belgium

18 E-mail: wout.boerjan@psb.vib-ugent.be

19 Telephone: + 32 (0)9 33 13 881

20

21

22 **ARTICLE TITLE**

23

24 ***cis*-cinnamic acid is a novel, natural auxin efflux inhibitor that promotes lateral root
25 formation**

26

27 **ALL AUTHORS NAME AND AFFILIATIONS**

28

29 Ward Steenackers^{1,2}

30 Petr Klíma³

31 Mussa Quareshy⁴

32 Igor Cesarino^{1,2,5}

33 Robert P. Kumpf^{1,2}

34 Sander Corneillie^{1,2}

35 Pedro Araújo^{1,2}

36 Tom Viaene^{1,2},

37 Geert Goeminne^{1,2}

38 Moritz K Nowack^{1,2}
39 Karin Ljung⁶
40 Jiří Friml⁷
41 Joshua J Blakeslee⁸
42 Ondřej Novák^{6,9}
43 Eva Zažímalová³
44 Richard Napier⁴
45 Wout Boerjan^{1,2,†,*}
46 Bartel Vanholme^{1,2,†,*}

47
48 ¹Department of Plant Systems Biology, VIB, B-9052 Gent, Belgium

49 ²Department of Plant Biotechnology and Bioinformatics, Ghent University, B-9052 Gent, Belgium

50 ³Institute of Experimental Botany, Czech Academy of Sciences, CZ-16502 Prague, Czech Republic

51 ⁴School of Life Sciences, University of Warwick, Coventry CV4 7AL, United Kingdom

52 ⁵Department of Botany, Institute of Biosciences, University of São Paulo, Butantã, São Paulo, Brazil

53 ⁶Umeå Plant Science Centre, Department of Forest Genetics and Plant Physiology, Swedish University of
54 Agricultural Sciences, SE-901 83 Umeå, Sweden

55 ⁷Institute of Science and Technology, Austria (IST Austria), 3400 Klosterneuburg, Austria

56 ⁸Department of Horticulture and Crop Science, the Ohio State University/OARDC, Wooster, OH 44691, USA

57 ⁹Laboratory of Growth Regulators, Centre of the Region Haná for Biotechnological and Agricultural Research,
58 Institute of Experimental Botany CAS and Faculty of Science of Palacký University, Šlechtitelů 27, CZ-78371
59 Olomouc, Czech Republic

60

61 †These authors contributed equally to this work and share last authorship.

62 *Corresponding authors. Bartel Vanholme; E-mail: bartel.vanholme@psb.vib-ugent.be; Telephone: + 32 (0)9 33
63 13 840. Wout Boerjan; E-mail: wout.boerjan@psb.vib-ugent.be; Telephone: + 32 (0)9 33 13 881.

64

65

66 **ONE SENTENCE SUMMARY**

67

68 The phenylpropanoid *cis*-cinnamic acid is natural auxin efflux inhibitor that promotes
69 lateral root formation

70

71 **LIST OF AUTHOR CONTRIBUTION**

72

73 WS designed the experiments, performed most of the experiments, analyzed the data and
74 wrote the article. PK performed the auxin accumulation assays. MQ performed auxin-binding

75 and anti-auxin experiments using Surface Plasmon Resonance (SPR), and did docking-
76 analysis. IC assisted in designing the experiments, provided technical assistance and
77 assisted in writing. SC and TV provided technical assistance with all experiments performed
78 with *Physcomitrella patens*. RPK and PA provided technical assistance with confocal imaging
79 and diverse phenotyping experiments, respectively. GG provided technical assistance on
80 ultra-performance liquid chromatography-mass spectrometry (UPLC-MS) and performed
81 data analysis. ON performed the auxin metabolite profiling. JJB performed the rootward
82 auxin transport assays using radiolabelled [³H]-IAA. KL, EZ and RN assisted in designing the
83 experiments and complemented the writing. MKN complemented the writing. JF and JJB
84 contributed to the experimental design and complemented the writing. BV and WB conceived
85 the project, assisted in designing the experiments, supervised the experiments, and wrote
86 the article.

87

88

89 **FUNDING INFORMATION**

90

91 This work has been supported by grants from the Hercules Foundation for the Synapt Q-ToF
92 (grant no. AUGE/014), by the Multidisciplinary Research Partnership 'Biotechnology for a
93 Sustainable Economy' (01MRB510W) of Ghent University and the Stanford University Global
94 Climate and Energy Project ('Lignin management: optimizing yield and composition in lignin-
95 modified plants'). SC is indebted to the Research Foundation Flanders for a predoctoral
96 (3G032912) fellowship. WS is indebted to the Agency for Innovation by Science and
97 Technology in Flanders (IWT) for a predoctoral fellowship. JF is supported by the European
98 Research Council (project ERC-2011-StG-20101109-PSDP). RK acknowledges the
99 OMICS@VIB post-doctoral program of the VIB. PK and EZ were supported by the Czech
100 Science Foundation (project no. 16-10948S) and EU Operational Programme Prague -
101 Competitiveness (project number CZ.2.16/3.1.00/21519), and ON acknowledges the Ministry
102 of Education, Youth and Sport of the Czech Republic (the National Program for Sustainability
103 I, grant no. LO1204). KL acknowledges the Swedish Governmental Agency for Innovation
104 Systems (VINNOVA) and the Swedish Research Council (VR). RN acknowledges the
105 support of BBSRC (BB/L009366), IC acknowledges the Foundation for Research of the State
106 of São Paulo (FAPESP) for the Young Investigators Awards research fellowship (grant
107 2015/02527-1). PA acknowledges Conselho Nacional de Desenvolvimento Científico e
108 Tecnológico (CNPq) fellowship (201998/2011-4).

109

110

111

112 **CORRESPONDING AUTHOR EMAIL**

113

114 bartel.vanholme@psb.vib-ugent.be

115 wout.boerjan@psb.vib-ugent.be

116

117

118 **ABSTRACT**

119 Auxin steers numerous physiological processes in plants making the tight control of
120 its endogenous levels and spatiotemporal distribution a necessity. This regulation is achieved
121 by different mechanisms including auxin biosynthesis, metabolic conversions, degradation
122 and transport. Here we introduce *cis*-cinnamic acid (*c*-CA) as a novel and unique addition to
123 a small group of endogenous molecules affecting *in planta* auxin concentrations. *c*-CA is the
124 photo-isomerization product of the phenylpropanoid pathway intermediate *trans*-CA (*t*-CA).
125 When grown on *c*-CA-containing medium, an evolutionary diverse set of plant species where
126 shown to exhibit phenotypes characteristic for high auxin levels, including inhibition of
127 primary root growth, induction of root hairs, and promotion of adventitious and lateral
128 rooting. By molecular docking and receptor binding assays, we showed that *c*-CA itself is
129 neither an auxin, nor an anti-auxin, and auxin profiling data revealed that *c*-CA does not
130 significantly interfere with auxin biosynthesis. Single-cell-based auxin accumulation assays
131 showed that *c*-CA, and not *t*-CA, is a potent inhibitor of auxin efflux. Auxin signaling reporters
132 detected changes in spatiotemporal distribution of the auxin response along the root of *c*-CA-
133 treated plants and long distance auxin transport assays showed no inhibition of rootward
134 auxin transport. Overall, these results suggest that the phenotypes of *c*-CA-treated plants are
135 the consequence of a local change in auxin accumulation, induced by the inhibition of auxin
136 efflux. This work reveals a novel mechanism how plants may regulate auxin levels and adds
137 a novel, naturally occurring molecule to the chemical toolbox for the studies of auxin
138 homeostasis.

INTRODUCTION

Plant growth and development are tightly regulated by a plethora of signaling compounds, which are present within the plant at extremely low concentrations. Although the molecular working mechanism for several of these compounds has been described in detail (phytohormones, such as auxin and cytokinin, being among the best studied), for others the underlying mode of action is still unknown. Cinnamic acid (CA) is one of them and whereas the first report on its biological activity dates back to 1935 (Haagen-Smit and Went, 1935; Hitchcock, 1935), little additional research has been performed on this compound.

CA is found *in planta*, both as *trans* (*t*)- and *cis* (*c*)-isomers, though not in equal concentrations (Yang et al., 1999; Yin et al., 2003). *t*-CA is synthesized through the deamination of phenylalanine by PHENYLALANINE AMMONIA-LYASE (PAL) after which it is hydroxylated to *p*-coumaric acid by CINNAMIC ACID-4-HYDROXYLASE (C4H) (Boerjan et al., 2003). These are the first steps of the general phenylpropanoid pathway that lead towards a plethora of secondary metabolites such as flavonoids, stilbenes, tannins and monolignols (Vogt, 2010) (Fig. S1). Besides being a crucial intermediate of an important pathway, *t*-CA itself has also been described as a bioactive compound, though its exact activity has remained a matter of debate. Depending on the experiment, *t*-CA has been described as inactive, anta- or agonistic to auxin or an inhibitor of polar auxin transport (Van Overbeek et al., 1951; Åberg, 1961; Letham, 1978; Liu et al., 1993). *c*-CA is a photo-isomerization product of *t*-CA and, in contrast to the latter, is detected only in trace amounts in plants (Yin et al., 2003; Wong et al., 2005). However, it has been suggested to have higher biological activity compared to *t*-CA (Haagen-Smit, 1935). *c*-CA inhibits the gravitropic response of etiolated tomato seedlings and young tomato plants (Yang et al., 1999) and promotes cell-elongation in *Pisum sativum* (Haagen-Smit and Went, 1935; Koepfli et al., 1938; Went, 1939) and epinastic curvature of tomato plants (Yang et al., 1999). Although these effects resemble, to some extent, the physiological effects caused by perturbed auxin or ethylene homeostasis, further studies claimed that the mode of action of *c*-CA might be different from that of auxin and independent of ethylene-signaling (Yang et al., 1999; Wong et al., 2005).

In addition to this inconsistent view on the physiological role of CA in plants, an adequate explanation concerning the molecular mechanism by which both isomers independently affect plant growth and development is lacking. We evaluated the working mechanism of CA and demonstrate that *t*-CA is inactive as a molecular signal, consistent with its role as a primary intermediate in the general phenylpropanoid pathway. In contrast,

174 its *c*-isomer is biologically active and acts as a natural inhibitor of cellular auxin efflux,
175 promoting lateral root formation.

177
178
179
180
181
182
183
184
185
186
187
188
189
190
191
192
193
194
195
196
197
198
199
200
201
202
203
204
205
206
207
208
209
210
211
212
213

RESULTS

1) CA affects plant development

An evolutionary diverse set of plant species was grown on tissue culture medium supplemented with commercially available CA and analyzed for aberrant growth phenotypes. In the higher land plants tested, CA inhibited primary root growth and induced the proliferation of adventitious and lateral roots in a dose-dependent manner (Fig. 1A and Supplemental Fig. S2A-D). In the Pteridophyte *Selaginella helvetica*, CA affected root apical meristem bifurcation, thickening of the root and root hair proliferation, resulting in a more dense root architecture (Supplemental Fig. S2E). In *Physcomitrella patens*, representing the Bryophytes, no clear effect on rhizoid growth was observed, but CA did stimulate cell and leaf elongation in the gametophores (Supplemental Fig. S2F-G). These results indicate that the addition of CA to the growth medium affects plant growth and development throughout the plant lineage.

To study the underlying molecular working mechanism of this compound we focused on *Arabidopsis thaliana*. In this model plant, the IC_{50-root} value (i.e. the CA concentration needed to reduce the primary root length by 50%) was determined to be 9.2 μM under the conditions tested (Fig. 1B). Lateral root formation and adventitious rooting were stimulated, and the overall increase in number of emerged lateral roots combined with the reduction in primary root length resulted in a considerable increase in lateral root density (LRD). A 1.4 and 2.5 fold increase in LRD was obtained at applied CA concentrations of 2.5 and 5 μM, respectively (Fig. 1C). Concentrations above 10 μM resulted in the outgrowth of fasciated lateral roots along the primary root, and a significant increase in the number of adventitious roots (Fig. 1D-E). Besides, an increase in root hair number and length was observed not only on the primary root (Fig. 1F), but also on the lateral roots (Fig. 1G). Finally, a root waving phenotype was observed in CA-treated plants (Fig. 1A), indicating gravitropism defect. This was confirmed in a bending assay, revealing a dose-dependent perturbation of the gravitropic response by CA (Fig. 1H).

All experiments were performed with pure *t*-CA; however, photo-isomerization towards its *c*-isomer could not be excluded during these experiments. The light-mediated isomerization of CA is well described and is induced by UV-B (Hocking et al., 1969). Although UV-B radiation (280-315 nm) was detected in the growth chamber, the intensity was low (~0.02 W/m²) and may not have been sufficient to increase the concentration of *c*-CA in the tissue culture medium during the growth period. To determine the isomerization efficiency under the applied plant growth conditions, 2.5 mg commercially available *t*- or *c*-CA was dissolved in 50 mL Milli-Q-H₂O/DMSO (80/20). Both solutions were subsequently placed in the growth chamber and the isomerization of both isomers was followed over time by ultra-high-pressure liquid chromatography (UHPLC)-mass spectrometry (MS). The chemical

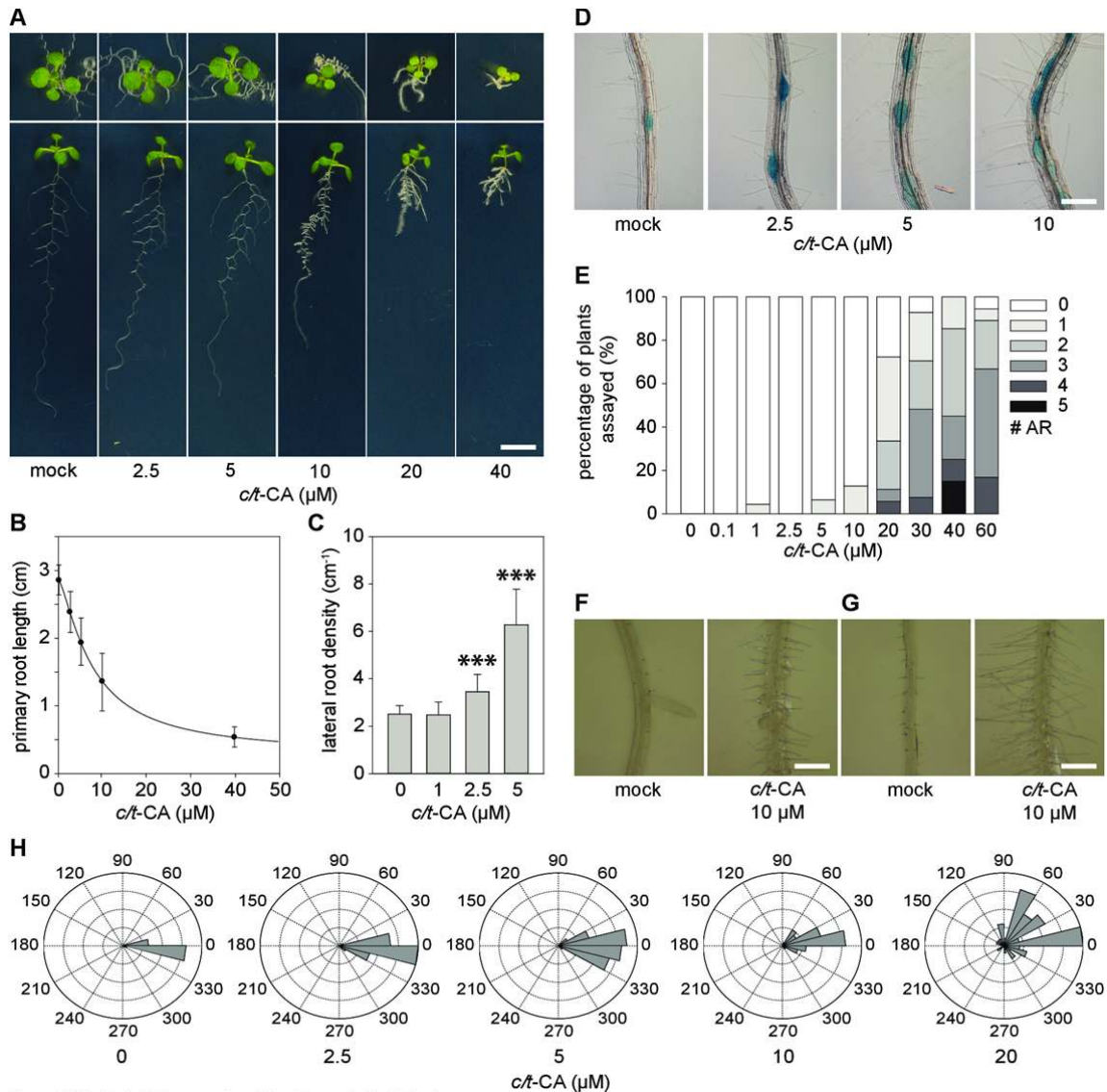


Figure 1. Effect of *c/t*-CA on growth and development of *Arabidopsis*.

(A) Root/rosette phenotype of representative seedlings 12 DAG, grown on 0.5xMS-medium supplemented with *c/t*-CA ($n > 20$ for each concentration) (scale bar: 1 cm). (B) *c/t*-CA dose response curve for primary root growth (Sigmoidal-logistic, 4 parameters) ($n > 20$). Error bars represent standard deviations. (C) Lateral root density of seedlings 12 DAG, grown on 0.5xMS-medium supplemented with *c/t*-CA ($n > 15$). Error bars represent standard deviations and asterisks were used to indicate statistically significant differences compared to the corresponding mock-treated control sample as determined by Dunnett's test P-values: * $P < 0.05$, ** $P < 0.001$, *** $P < 0.0001$. (D) Representative light microscopic images of a root segment with lateral root primordia visualized by *CYCB1:GUS* expression in *Arabidopsis* 12 DAG of seedlings grown on 0.5xMS-medium supplemented with different concentrations of *c/t*-CA ($n > 10$) (scale bar: 0.5 cm). (E) Number of adventitious roots of seedlings 12 DAG grown on 0.5xMS-medium supplemented with *c/t*-CA. Plants were grown for 7 days in darkness (after a short light-pulse of 4h with red-light to induce germination) and subsequently transferred to light to stimulate adventitious rooting. Adventitious root numbers are represented in grey-scale ($n > 20$). (F-G) Binocular microscopic images of a root segment of the (F) primary root and (G) lateral root of seedlings 12 DAG, grown on 0.5xMS-medium whether or not supplemented with 10 μ M *c/t*-CA ($n = 10$). (H) Histogram showing the *c/t*-CA-induced disruption of the gravitropic response in the main root. Seeds were germinated on 0.5xMS-medium and 4 DAG seedlings were transferred to 0.5xMS-medium supplemented with *c/t*-CA. Subsequently, seedlings growing on vertical plates were rotated 90 degrees and each root was assigned to one of 12 30° sectors after 48h incubation ($n > 25$).

214 equilibrium was in favor of the *c*-isomer (57%) and was reached after 8 or 15 days,
 215 depending on the use of *c*-CA or *t*-CA as the initial compound (Supplemental Fig. S3). This
 216 indicates that despite the application of *t*-CA to the growth medium, a substantial amount of
 217 the *c*-isomer could be expected during the period of plant growth. Consequently, the
 218 observed growth defects could not be linked unambiguously to the presence of *t*-CA in the
 219 medium.

220 No spontaneous isomerization was detected in the dark, under deep-red (650-
 221 670nm), or far-red illumination (725-750nm). Therefore, experiments to reveal the effect of

222 the pure isomers could be performed under these conditions. To distinguish the experiments
223 performed with *t*-CA in the dark from experiments performed in the light, the latter will be
224 indicated as *t/c*-CA here onwards, although *t*-CA was added to the tissue culture medium for
225 both experiments.

226 Knowing the photo-isomerization conditions, we questioned if both isomers had
227 similar biochemical properties. Arabidopsis seeds were placed on 0.5×MS-medium
228 supplemented with either pure *c*-CA or *t*-CA and incubated in darkness to avoid photo-
229 isomerization. Twelve days after germination (DAG) seedlings were screened for phenotypes
230 as before. Whereas no effect on the elongation of the hypocotyl was observed (Fig. 2A), an
231 inhibitory effect on primary root growth was evident (Fig. 2B). Here *c*-CA was much more
232 effective than *t*-CA (IC_{50-root} of 3.2 μM and 82.4 μM for *c*- and *t*-CA, respectively). To test the
233 metabolism of *t*- versus *c*-CA, a yeast heterologous expression system was used to express
234 Arabidopsis C4H. In contrast to *t*-CA, *c*-CA was not converted to *p*-coumaric acid by
235 Arabidopsis C4H (Supplemental Fig. S4).

236 Therefore, only *t*-CA is an intermediate in the general phenylpropanoid pathway. The
237 *c*-isomer is the biologically active isomer affecting a number of developmental processes *in*
238 *planta* and it is likely that most if not all physiological effects that have been previously
239 attributed to the *t*-CA isomer or CA in general, are caused by *c*-CA.

240

241 **2) c-CA affects root architecture**

242 In Arabidopsis, lateral roots arise from asymmetric anticlinal divisions of founder cells
243 in the pericycle layer basal to the main root meristem (De Rybel et al., 2010). As *c*-CA
244 causes lateral root proliferation (Fig. 1D), the effect of *c*-CA on cell division in this cell layer
245 was studied in more detail using the cell plate marker KNOLLE. An increase in the
246 expression of *KNOLLE*-driven *GFP* was observed along the pericycle of 7 day old dark-
247 grown seedlings treated for 3 days with 10 μM *c*-CA, confirming strong induction of mitotic
248 activity in this cell layer upon addition of *c*-CA (Fig. 2C). Notably, prolonged treatment for 3
249 days with 10 μM *c*-CA resulted in epidermal and cortical cell peeling (Fig. 2C) suggesting
250 active degradation of the pectin-rich middle lamella between adjacent cells.
251 POLYGALACTURONASE ABSCISSION ZONE ARABIDOPSIS THALIANA (*PGAZAT*)
252 mediated pectin degradation is known to be important for lateral root outgrowth (Gonzalez-
253 Carranza et al., 2007; Kumpf et al., 2013) and the *PGAZAT* promoter turned out to be
254 strongly activated by 10 μM *c*-CA in cortical and epidermal cell layers surrounding developing
255 lateral roots, but not in the lateral roots themselves (Fig. 2D). The active cell wall remodeling
256 in the epidermis and cortex will facilitate the outgrowth of the *c*-CA induced lateral roots.

257 Both the *KNOLLE* and *CYCB1* reporter lines highlighted the effect of *c*-CA on the left-
258 right alternation and spatial organization characteristic for Arabidopsis lateral roots (Fig. 1D)

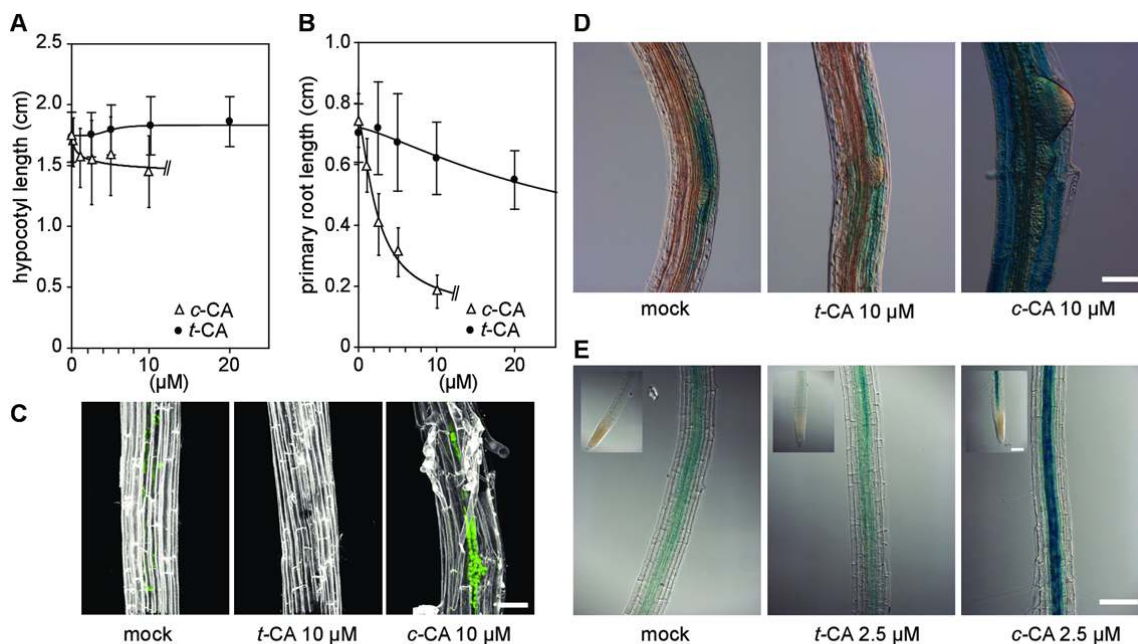


Figure 2. Effect of *c*-CA on root architecture.

Dose response curves (Sigmoidal-logistic, 4 parameters) showing the effect of *c*-CA (triangles) or *t*-CA (dots) on (A) hypocotyl and (B) root length of seedlings 12 DAG, grown in darkness on 0.5xMS-medium supplemented with either *c*- or *t*-CA ($n > 20$). Seed germination was induced by a 4h red light-pulse. (C) Confocal images showing *KNOLLE* promoter activity (green) of 10 DAG *pKNOLLE:KNOLLE-GFP* seedlings. (D-E) Light microscopic images of *c*-CA induced GUS activity in 10 DAG *pPGAZAT:GUS* and *pGATA23:GUS* seedlings. GUS activity was monitored at the lateral roots (*PGAZAT*) or the zone basal to the main root tip (*GATA23*). For the *GATA23* driven GUS expression the main root tip is shown as inset. For (C) and (D), seeds were germinated on 0.5xMS-medium and 7 DAG seedlings were transferred to 0.5xMS-medium supplemented with 10 μ M *c*-CA or *t*-CA ($n=5$) (scale bar: 15 μ m). Growth conditions for (E) were as for (C) with the only exception that *c*-CA and *t*-CA were used at 2.5 μ M ($n=5$).

259 and Fig. 2C). The altered root pattern could originate at the level of lateral root founder cell
 260 specification, which occurs in the basal meristem before the initial anticlinal division of the
 261 founder cells (De Rybel et al., 2010). To visualize the effect of *c*-CA on lateral root priming
 262 we used a reporter line harboring the promoter of the *GATA23* transcription factor fused to a
 263 *GUS* reporter. *GATA23* expression is considered as hallmark of the earliest steps in lateral
 264 root formation (De Rybel et al., 2010). In mock-treated plants, *GUS* expression was observed
 265 in pericycle cells starting close to the root tip and continued along the root in a zone lacking
 266 emerged lateral root primordia. Treating the marker line 5 days after germination (DAG) with
 267 2.5 μ M *c*-CA for 21 hours resulted in ectopic and enhanced GUS activity stretching
 268 continuously from the main root tip onwards till the maturation zone. In addition, local
 269 patches of strong GUS activity were observed, most likely corresponding to founder cell
 270 formation in pericycle cells adjacent to xylem pools (Fig. 2E and Supplemental Fig. S5).

271 These results reveal that *c*-CA triggers cell priming, which initiates lateral root
 272 proliferation. *t*-CA included in each set of experiments for comparison, never induced an
 273 effect different from the mock-treatment, supporting our previous finding that the biological
 274 activity of CA is restricted to its *c*-isomer.

275

276 3) *c*-CA triggers an auxin response

277 Lateral root proliferation is a classical auxin-mediated process. To disclose putative
 278 crosstalk between *c*-CA and auxin, we monitored whether *c*-CA could affect the local auxin

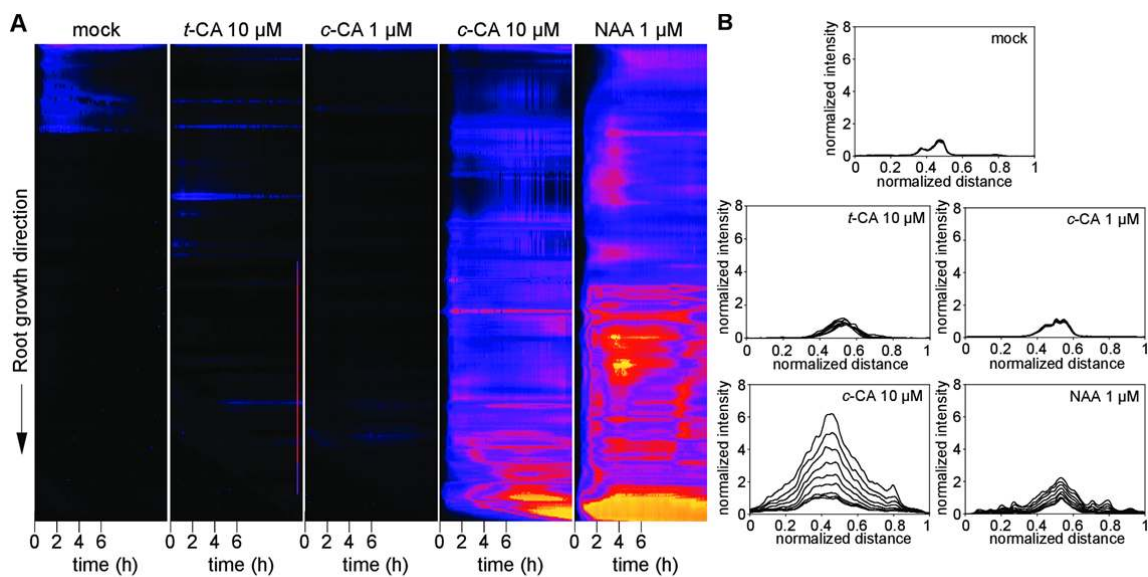


Figure 3. *c*-CA induces an auxin response in Arabidopsis.

(A) Kymograph of *pDR5:LUC* intensity along the primary root of Arabidopsis seedlings during a 12h period. The kymograph represents on the vertical axis the primary root, with the root tip present in the origin of the coordinate system, and the shoot/root junction at the end of the vertical axis. The horizontal axis represents time. Seeds were germinated on 0.5xMS-medium and 5 DAG seedlings were transferred to 0.5xMS-medium supplemented with 1-10 μ M *c*-CA, 10 μ M *t*-CA or 1 μ M NAA. Imaging was started at the moment of transfer and data was recorded every 10 minutes. Each kymograph represents one experiment. The kymograph is representative for 8 biological repeats (seedlings). B) Confocal time-lapse imaging of *pDR5rev:GFP* intensity in the primary root between two young emerged lateral roots. At the start of the time-lapse, seedlings were placed in glass-bottomed dishes and covered with 0.5xMS-medium containing 1 μ M NAA, 1-10 μ M *c*-CA or 10 μ M *t*-CA. The time-lapse was started 5 minutes after the seedlings had been placed in contact with the media and captured every 60 minutes over a 16h period. Cumulative spectra were obtained by projecting the GFP intensity on a virtual line crossing the middle of the primary root. Normalization was performed against the maximal intensity of the signal at the earliest time point ($n=1$). Each spectrum is representative for 3 biological repeats (positions along the primary root).

279 response along the primary root using the auxin response reporter *DR5:LUC* (Moreno-
 280 Risueno et al., 2010). Arabidopsis seedlings were transferred 5 DAG to 0.5xMS-medium
 281 supplemented with the compound of interest and luciferase activity was monitored every 10
 282 minutes over a 12h time interval. In mock-treated plants, luciferase activity was seen in the
 283 shoot/root apical meristems, and lateral root initiation sites. This spatial pattern is in line with
 284 the described distribution of auxin maxima along the primary root of Arabidopsis seedlings
 285 (Benkova et al., 2003). Supplying the medium with 10 μ M *t*-CA did not affect this pattern,
 286 whereas the addition of 1 μ M naphthalene-1-acetic acid (NAA) resulted in a strong increase
 287 in luciferase activity along the primary root from the first time point onwards, and the signal
 288 intensity increased over time (Fig. 3A and Supplemental Fig. S6). Similar to NAA, *c*-CA
 289 caused an increase in the luciferase signal in a dose-dependent manner. When supplied at
 290 10 μ M, the signal accumulated along the primary root. However, after 6 hours the luciferase
 291 activity dropped in the root maturation zone, but remained in the lateral root primordia and
 292 the primary root tip, where the signal accumulated to saturation levels. This spatial
 293 distribution was highly similar to that obtained with a lower *c*-CA dose (5 μ M), although the
 294 whole process was slower and never reached saturation during the timespan of the
 295 experiment. (Fig. 3A and Supplemental Fig. S6).

296 Besides the spatial shift of the *c*-CA-induced *DR5*-driven signal along the longitudinal
 297 axis of the root, an axial redistribution of the signal was observed as well. To follow and
 298 quantify this lateral distribution over time we shifted to 4D microscopy using *DR5rev:GFP*

299 seedlings (Friml et al., 2003), grown and treated as for the *DR5:LUC* experiment. After
300 transferring seedlings 5 DAG to the *c*-CA-containing medium (10 μ M), the region between
301 two young emerged lateral roots was scanned every hour over a 16h period. At the second
302 time point (2h) a significant increase in fluorescence was observed in the stele, increasing
303 with time, and expanding across the pericycle into neighboring cell layers (Fig. 3B and
304 Supplemental Fig. S7). A comparable pattern was obtained with 1 μ M NAA (included as
305 positive control), although the fluorescence at the end of the observation period was lower as
306 compared to that achieved with *c*-CA-treated roots (Fig. 3B and Supplemental Fig. S7).

307 These observations show that *c*-CA has auxin-like effects on plant development and
308 affects the spatial distribution of the auxin response at low micro molar concentrations.

309

310 **4) *c*-CA does not act as a typical auxin**

311 The overall similarity in *DR5*-driven fluorescence between *c*-CA- and NAA-treated
312 plants suggests that *c*-CA functions via the TRANSPORT INHIBITOR RESPONSE1/AUXIN
313 SIGNALING F-BOX (TIR1/AFB) auxin-signaling pathway (Peret et al., 2009). To investigate
314 whether *c*-CA acts via this canonical auxin-signaling pathway, we grew the *solitary root-1*
315 (*slr*) gain-of-function Aux/IAA mutant and the *arf7 arf19* double mutant on *c/t*-CA-
316 supplemented medium. Like auxin, *c/t*-CA failed to induce lateral root formation in these
317 mutants, suggesting that *c*-CA functions upstream of these steps in the auxin signaling
318 cascade toward lateral root formation (Fig. 4A). As SLR1/IAA14 is a direct target of the auxin
319 receptor TIR1, we subsequently tested whether TIR1 was essential for *c*-CA activity by
320 growing the *tir1 afb2 afb3* mutant on *c/t*-CA containing medium. As for the other mutants
321 tested no lateral roots were induced in this mutant indicating that the TIR1 auxin receptor is
322 crucial for this *c*-CA-mediated growth defect (Fig. 4A). Based on these observations we
323 concluded that *c*-CA could be an auxin analogue that induces the auxin signaling cascade by
324 interacting with the TIR1 auxin receptor in a similar way as the native auxin, indole-3-acetic
325 acid (IAA). However, simulation of the molecular docking of *c*-CA in the auxin receptor
326 pocket of TIR1 revealed a position different from the experimentally determined orientation of
327 IAA (Supplemental Fig. S8). To validate the prediction, the interaction kinetics of TIR1 and
328 the related AFB5 with immobilized peptides corresponding to the degron motif of Aux/IAA7
329 were followed using Surface Plasmon Resonance (SPR). Whereas strong signals were
330 obtained with IAA and NAA used as a positive controls, no evidence for a specific binding of
331 *c*-CA or *t*-CA to the auxin receptors was found (Fig. 4B). Both isomers were also tested for
332 anti-auxin activity. Although such property was claimed for *t*-CA (Van Overbeek et al., 1951),
333 no supporting evidence for such activity was found (Fig. 4B).

334 Together, these results indicate that neither CA-isomer acts as an auxin agonist, nor
335 an antagonist at the level of the auxin perception and support the hypothesis that *c*-CA acts

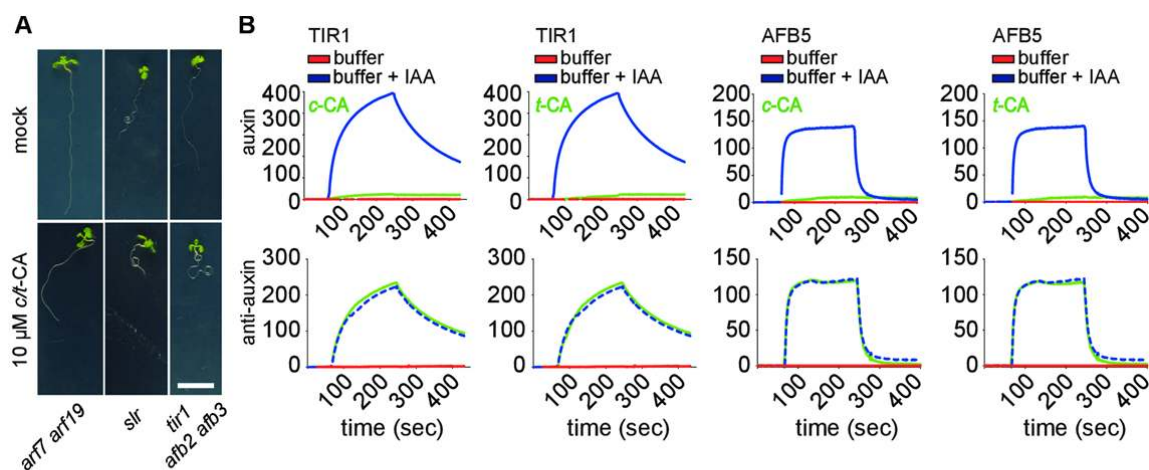


Figure 4. *c*-CA does not act as a typical auxin.

(A) Root phenotype of *arf7 arf19*, *slr* and *tir1 afb2 afb3* mutants 12 DAG, growing on 0.5xMS medium supplemented with 10 μ M *c*-CA ($n > 25$) (scale bar: 1 cm). (B) Surface Plasmon Resonance sensorgrams showing the auxin-dependent interaction between TIR1 or AFB5 with IAA DII. Each sensorgram shows the binding with IAA (blue), an auxin-free injection (red) plus the data for each test compound (green). For auxin activity assays (top) compounds (50 μ M) were mixed with TIR1 or AFB5 prior to injection over DII peptide. For anti-auxin assays (bottom), compounds (50 μ M) were mixed with TIR1 or AFB5 plus 5 μ M IAA prior to injection. The degron sequence that was used: biot-AKAQVVGVPPVVRNYRKN.

336 via an auxin-dependent pathway for lateral root formation by modifying auxin homeostasis or
 337 the spatiotemporal distribution of auxin in roots.

338

339

5) *c*-CA triggers lateral root formation in an auxin-dependent manner

340

341

342

343

344

345

346

347

348

349

350

351

352

353

354

355

356

357

358

359

To assess whether activation of the *DR5* promoter is due to an overall shift in IAA concentrations, UHPLC-MS profiling was performed on Arabidopsis seedlings 12 DAG. Before the extraction plants were treated with 10 μ M *c*-CA or *t*-CA for 1 and 6 hours (Supplemental Fig. S9 and S10). No major shifts in the IAA metabolome were observed between *t*-CA- and mock-treated plants again confirming the absence of bioactivity for this compound. For the *c*-CA-treatment an effect was observed 6 hours after the transfer of the seedlings to 10 μ M *c*-CA (Supplemental Fig. S10). At this point a small, but significant increase in indole-3-acetamide, indole-3-acetonitrile, and indole-3-acetaldoxime was observed. In addition, intermediates of the indole-3-pyruvic acid (IPyA)-pathway for IAA biosynthesis accumulated in seedlings treated with *c*-CA for 6 hours. This pattern could be transient as no significant increase in free IAA levels or in any of its conjugates was detected after 6 hours. The absence of a clear shift in free IAA levels in combination with the observed rapid and strong activation of the *DR5* promoter questions the importance of auxin biosynthesis for *c*-CA-induced lateral root formation. The role of IAA itself was reconsidered by testing lateral root induction in plants with artificially reduced IAA levels using the IAA lysine synthase (*iaaL*) overexpressing line. The bacterial *IAAL* gene encodes an enzyme which inactivates IAA by conjugating it to the amino-acid lysine. Seeds from the *p35S:iaaL*-line were germinated as above and LRD was quantified 12 DAG. When treated with *t*-CA, *p35S:iaaL* plants showed fewer lateral roots than WT plants, indicating that *c*-CA-induced lateral root induction is indeed mediated by free IAA (Supplemental Fig. S11).

360 In summary, the bioactivity of *c*-CA is clearly dependent on auxin. The fact that free
361 IAA is not increased in *c*-CA-treated plants suggests that auxin is redistributed within the
362 plant, resulting in novel auxin maxima that inhibit primary root growth and promote lateral
363 root development.

364

365 **6) *c*-CA inhibits cellular auxin efflux**

366 The ability of *c*-CA to induce an auxin response via the canonical auxin-signaling
367 pathway without being a receptor agonist suggests that *c*-CA interferes with tightly controlled
368 auxin concentrations in the plant. To obtain insight into possible *c*-CA-mediated dynamic
369 changes of auxin responses at high spatial resolution in a short time-interval the visual
370 marker DII-VENUS was used (Brunoud et al., 2012). A time-course was recorded of DII-
371 VENUS fluorescence in the primary root tip of Arabidopsis seedlings 7 DAG. Forty-five
372 minutes after the addition of 1 μ M NAA DII-VENUS fluorescence dropped to 25% of its initial
373 intensity (Fig. 5A and Supplemental Fig. S12), which is in line with previously published data
374 (Brunoud et al., 2012). The DII-VENUS sensor reacted in a similar way following treatment
375 with *c*-CA, although compared to NAA a 10-fold higher concentration of *c*-CA was required to
376 reduce the fluorescence to a comparable level (i.e. 29% of the initial fluorescence after 42
377 minutes with 10 μ M *c*-CA; Fig. 5A and Supplemental Fig. S12). Remarkably, also *t*-CA turned
378 out to be active in this assay, which contradicts previous findings claiming activity restricted
379 to the *cis*-isoform. However, the *t*-CA mediated reduction of DII-VENUS signal is most likely
380 a direct consequence of laser mediated isomerization of *t*-CA towards *c*-CA during imaging
381 (so called photo-activation). Lowering the concentration of *c*-CA to 1 μ M resulted in a pattern
382 indistinguishable from that of mock-treated samples during the initial time points. Intriguingly,
383 after 10 minutes the pattern started to deviate from the negative control and a slight increase
384 in DII-VENUS degradation could be observed. This trend was sustained and resulted in a
385 significant drop in fluorescence by the end of the experiment. Interestingly, DII-VENUS
386 degraded at a similar speed as in the samples treated with the higher concentration of *c*-CA
387 (Fig. 5A). This peculiar profile could indicate that *c*-CA interferes with auxin transport. This
388 would lead to increasing intracellular auxin concentrations and consequent DII-VENUS
389 degradation once a critical auxin concentration threshold is passed. To find supporting
390 evidence for this hypothesis the experiment was repeated with 1-naphthylphthalamic
391 acid (NPA), a well-established inhibitor of auxin efflux. As for *c*-CA, NPA caused a dose-
392 dependent reduction in DII-VENUS fluorescence with similar dynamics as after treatment
393 with *c*-CA, indicating that both these compounds similarly increase auxin accumulation in the
394 primary root tip (Supplemental Fig. S13). In line with the proposed model, at the lower
395 concentrations tested (0.1 and 1.0 μ M NPA), a pattern was obtained which only deviated

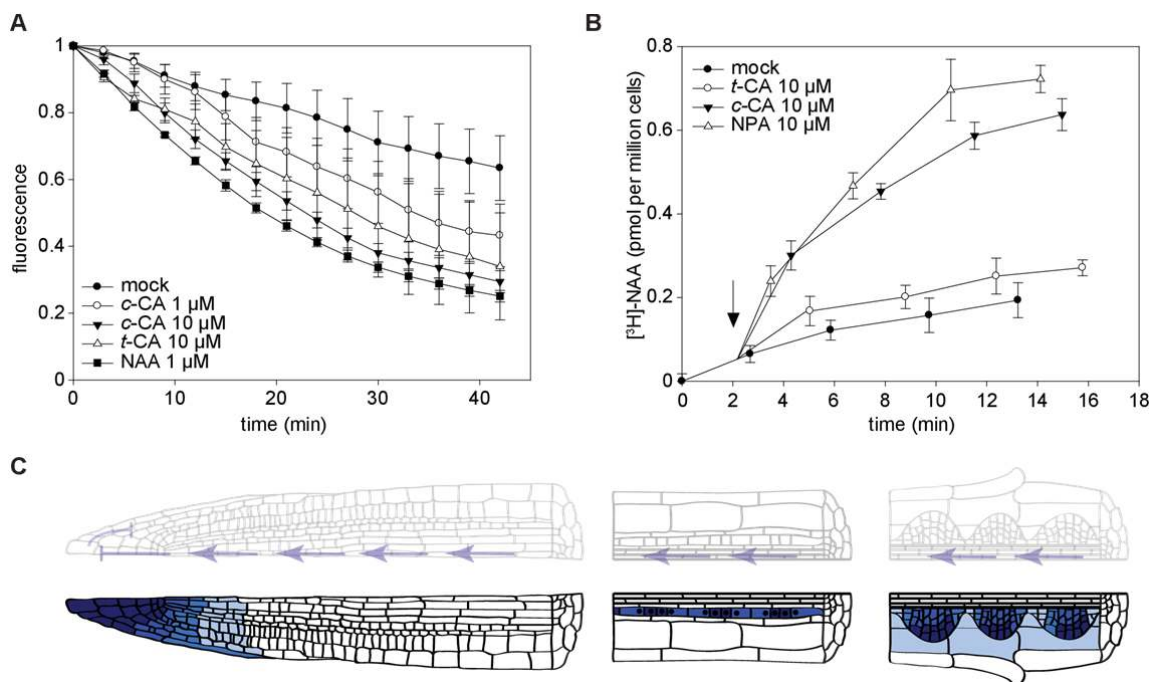


Figure 5. Effect of *c*-CA on polar auxin transport.

(A) Time-course of DII1-VENUS fluorescence in the main root tip of *DII1-VENUS-YFP* seedlings. Plants were germinated on 0.5xMS-medium and subsequently transferred 5 DAG to 0.5xMS-medium supplemented with 1 or 10 μ M *c*-CA, 10 μ M *t*-CA or 1 μ M 1-NAA ($n=3$). (scale bar: 50 μ m). Fluorescence was quantified every 3 minutes over a 42 minute period. During each experiment 3 root tips (representing one treatment) were simultaneously imaged. Error bars represent standard deviations. (B) Effect of 10 μ M *c*-CA, *t*-CA or NPA on the net accumulation of [3 H]-NAA in 2-day old suspension-cultured tobacco BY-2 cells (20 minute uptake period). The arrows points to the time of application of the compound. Error bars represent standard deviations ($n=4$). (C) Model explaining the *c*-CA mediated lateral root proliferation. *c*-CA inhibits shootward auxin transport by inhibiting the redistribution of auxin in the meristem. This is considered a direct consequence of the *c*-CA mediated inhibition of auxin efflux. The phloem-mediated rootward auxin transport in the primary root is not disturbed by *c*-CA, allowing a continuous supply of auxin from the shoot towards the root tip. The block of a proper auxin redistribution in the meristem results in the accumulation of auxin in the primary root, where it triggers lateral root proliferation. Top: auxin flow (blue arrows) and its perturbation within the primary root of *c*-CA treated plants. Bottom: schematic representation of auxin accumulation in the primary root of *c*-CA treated plants and the consequent induction of lateral roots.

396 from the mock-treated control after a temporal delay, of which the length was dependent on
 397 the NPA concentration (Supplemental Fig. S13).

398 The putative link between *c*-CA and polar auxin transport machinery was further
 399 explored by auxin accumulation assays on the cellular level. Polar auxin transport depends
 400 on the localization and activity of auxin influx and efflux carriers (Adamowski and Friml,
 401 2015). In tobacco cells, NAA enters the cells mainly by diffusion (Delbarre et al., 1996;
 402 Hoyerova et al., 2011), whereas it is an excellent substrate for active efflux. Therefore, a
 403 change in intracellular accumulation of radioactively-labeled NAA in BY-2 tobacco cell-
 404 suspension culture over time provides a measure of the activity of auxin efflux from cells (Fig.
 405 5B). Control cells displayed [3 H]-NAA accumulation kinetics indicative of active and saturable
 406 auxin-efflux (Petrasek et al., 2006). After treatment with NPA [3 H]-NAA accumulated strongly
 407 inside the cells, and a similar although slightly reduced response was obtained when NPA
 408 was replaced with *c*-CA, indicating that *c*-CA acts as a potent inhibitor of auxin efflux. This
 409 increase in accumulation was not observed upon treatment with *t*-CA (Fig. 5B). When a
 410 similar experiment was performed with a combination of NPA and *c*-CA, [3 H]-NAA
 411 accumulated to a similar level as in NPA-treated cells, indicating *c*-CA targets a subset of
 412 NPA-sensitive auxin transporters (Supplemental Fig. S14), which could be either PIN-
 413 FORMED (PIN) or ATP-binding cassette-B (ABCB) transporters (Petrasek et al., 2009). To

414 distinguish between both, NPA was substituted for the ABCB-specific inhibitor 2-[4-
415 (diethylamino)-2-hydroxybenzoyl] benzoic acid (BUM) (Kim et al., 2010). In contrast to NPA,
416 BUM inhibited auxin efflux to the same extent as *c*-CA in the auxin transport assay, and no
417 additive effect was observed when BUM and *c*-CA were used simultaneously (Supplemental
418 Fig. S15). This strongly suggests *c*-CA targets predominantly the ABCB-auxin transport
419 machinery. To test whether *c*-CA might also affect auxin influx, [³H]-NAA was replaced for
420 [³H]-2,4-D, which is a preferred substrate for influx activity. When added to the BY-2 cell
421 suspension, [³H]-2,4-D accumulated in the cells until a plateau was reached, representing
422 equilibrium between cellular influx and efflux of the labeled compound (Supplemental Fig.
423 S16). Using this experimental setup we found no indication that either *c*-CA or *t*-CA affects
424 cellular auxin influx.

425 Based on these experiments, we concluded that *c*-CA, but not *t*-CA, inhibits auxin
426 efflux from cells, more specifically the ABCB-mediated part of auxin efflux. The consequent
427 accumulation of intracellular auxin could be at the basis of the physiological and
428 developmental defects observed in *c*-CA-treated Arabidopsis seedlings.

429

430 **7) *c*-CA does not inhibit long-distance rootward auxin transport**

431 Although both NPA and *c*-CA block cellular auxin efflux, their effects on Arabidopsis
432 roots are entirely different. NPA arrests (Casimero et al., 2001; Benkova et al., 2003) and *c*-
433 CA induces lateral root formation. Supported by the spatiotemporal distribution of *DR5* driven
434 luciferase activity we hypothesized that a difference in long-distance auxin transport could be
435 the origin of the phenotypic difference between these two auxin efflux inhibitors. Whereas
436 NPA affects both rootward and shootward auxin transport in the primary root (Casimero et
437 al., 2001), the strong increase in luciferase activity in the tip of *c*-CA-treated roots suggested
438 that rootward auxin transport is not disturbed by *c*-CA. To verify this hypothesis, we
439 monitored whether local *c*-CA application could affect distant auxin-inducible luciferase
440 activity using a split medium approach as described by Lewis and Muday (2009). To this end,
441 seedlings were positioned on the medium in a way that either the upper or the lower half of
442 the root was in contact with *c*-CA. Dynamics of luciferase activity along the root were
443 followed over time as described above. When the lower half of the root was in contact with *c*-
444 CA, luciferase activity accumulated in the root tip in line with earlier data (Supplemental Fig.
445 S17). When only the upper part of the root was in contact with *c*-CA, the luciferase signal
446 quickly extended towards the non-treated zone (Supplemental Fig. S17). This illustrates that
447 auxin appears to be able to pass through the *c*-CA-treated zone in a rootward direction.

448 Although the data support the hypothesis that *c*-CA allows long-distance rootward
449 auxin transport, we could not exclude an alternative explanation, namely that *c*-CA itself is
450 transported and triggers auxin signaling locally. To provide undisputed evidence for rootward

451 transport of auxin in *c*-CA treated roots, long-distance rootward auxin transport was assayed
452 in primary roots of Arabidopsis seedlings in which the roots were exposed to either mock or
453 *c*-CA-treated 0.5xMS-medium. In these assays, microdroplets of radiolabelled [³H]-IAA were
454 placed precisely on the shoot apical meristems of Arabidopsis seedlings and rootward auxin
455 transport was measured by harvesting a 4 mm segment centered on the root/shoot transition
456 zone, as well as the entire root, in 2 mm segments. Consistent with previous results,
457 treatment with *c*-CA did not inhibit rootward auxin movement (Fig. 5C and Supplemental Fig.
458 S18). The strong accumulation of the auxin-inducible luciferase in the root tip is characteristic
459 of the inhibition of shootward auxin transport (Fig. 3A and Supplemental Fig. S6 and S17).
460 Unfortunately, reliable data were not obtained for shootward auxin transport to support this
461 hypothesis.

462 Taken together, our data supports a model (Fig. 5C) in which *c*-CA inhibits auxin
463 efflux at the cellular level in specific cells at or near the root apical meristem, while allowing
464 long-distance rootward auxin transport at the organ level. The resultant accumulation of
465 auxin in the root apical meristem might cause, at least in part, the observed growth defects
466 induced by *c*-CA.

467

468
469
470
471
472
473
474
475
476
477
478
479
480
481
482
483
484
485
486
487
488
489
490
491
492
493
494
495
496
497
498
499
500
501
502
503
504

DISCUSSION

Being sessile organisms, plants cannot escape unfavorable growth conditions. This shortcoming is compensated by an extreme plasticity allowing them to react on changing environmental cues. Here, the phytohormone auxin has an important function as it is key in the regulation of many processes involved in growth and development (Vanneste and Friml, 2009). As for all bioactive compounds, tight regulation of its homeostasis and spatiotemporal distribution inside the plant is crucial, as suboptimal auxin concentrations will not trigger the desired response, while high concentrations will be harmful. The ability to control auxin levels is a necessity for plant survival and occurs at the cellular level by regulating biosynthesis, metabolic conversions as well as degradation, whereas transport is essential to translocate auxin between different cells and tissues. Synthetic inhibitors of auxin transport such as NPA and BUM have proven the importance of this process in diverse physiological actions, including embryogenesis, tropisms, vascular patterning and lateral root initiation (Kim et al., 2010). Intriguingly, endogenous auxin transport inhibitors are scarce. Flavonols and flavonoids such as quercetin were considered to inhibit auxin transporters (Brown et al., 2001) although later work suggested that flavonoids also act by redirecting PIN efflux protein localization (Santelia et al., 2008). Certain flavonoid mutants display auxin-related defects (Buer et al., 2013) and an auxin-transport inhibiting activity was recently assigned to the flavonol glycoside kaempferol 3-*O*-rhamnoside-7-*O*-rhamnoside (Yin et al., 2014).

Here we introduce *c*-CA as a novel endogenous inhibitor of auxin transport. Intriguingly, the activity of *c*-CA resembles that of NPA but only at the cellular level. Although both NPA and *c*-CA block cellular auxin efflux, the effects of the two compounds on *Arabidopsis* root architecture are entirely different, with *c*-CA inducing lateral root formation and NPA impacting several auxin-dependent phenotypes, including lateral root initiation. The exact mechanism of NPA action is still unknown, but according to one hypothesis the *solitary root* phenotype of NPA-treated plants is a consequence of auxin depletion in the root due to the perturbation of basipetal and acropetal auxin transport (i.e. shootward and rootward, respectively) (Casimiro et al., 2001). While, explaining the observed phenotype, the molecular mechanism underlying the inhibition of phloem-based (and hence no-transporter mediated) rootward auxin transport by an auxin efflux inhibitor remains unknown. Proceeding from this model we hypothesized that a difference at the level of rootward transport (blocked by NPA but not by *c*-CA) underlies the phenotypic differences caused by the two compounds. Under mock conditions, auxin is redistributed in the root tip according to the “reverse-fountain” model, in which specific auxin transport proteins (PINs and ABCB proteins) play distinct roles in establishing directional movement of auxin (Benkova et al., 2003; Bliilou et al., 2005; Lewis and Muday, 2009). By inhibiting cellular auxin efflux, we hypothesize *c*-CA will affect the auxin reflux in the meristem resulting in the inhibition of

505 shootward auxin transport. Consequently, auxin either transported from the shoot or
506 synthesized in the primary root tip will accumulate behind the root tip where it will trigger
507 GATA23-expression and affect lateral root founder cell specification. Over time, the
508 accumulating auxin will enter pericycle cells, either by diffusion or active influx where it will be
509 trapped due to the *c*-CA mediated inhibition of auxin efflux, similar to the situation in the
510 primary root. Once the auxin concentration passes a critical threshold, primed cells will be
511 triggered to develop into lateral root founder cells, which eventually will develop into new
512 lateral roots, shaping the altered root architecture (Fig. 5C).

513 Compared to NPA, *c*-CA was found slightly less efficient in the auxin accumulation
514 assay. This difference may result from the broader specificity of NPA, known to affect
515 different types of auxin efflux carriers. Based on the absence of an additive effect of *c*-CA
516 and BUM in this assay we concluded that *c*-CA targets the ABCB subfamily of the multi-drug
517 resistant/P-glycoprotein (MDR/PGP) integral membrane proteins. These transporters are well
518 known for their capacity to pump drugs out of the cell (Kang et al., 2011), increasing the
519 resistance of the cell and hence the organism towards compounds that are considered toxic
520 under normal conditions. Interestingly, and in line with our observation, the *cis*-form of CA
521 and not its *trans*-form raises a notable synergistic bactericidal activity against multiple-drug
522 resistant *Mycobacterium tuberculosis*. It is tempting to speculate that also in this case *c*-CA
523 blocks the MDR-transporters, resulting in the intracellular accumulation of the supplied
524 antibiotics to levels required to kill the bacteria (Chen et al., 2011).

525 Although the physiological role of endogenous *c*-CA is still unclear, the beauty of this
526 bioactive molecule lies in the fact that it can be produced from a readily available inactive
527 compound (*t*-CA) by sunlight (Ding et al., 2011). This gives a tremendous opportunity to link
528 environmental conditions directly to developmental regulation without the need to activate
529 gene expression to alter the auxin pool. In addition, we cannot exclude that a similar
530 conversion can be obtained by a yet-to-be-discovered enzyme, further extending the
531 possibilities to exploit this mechanism to steer plant development independently of light. The
532 question of whether or not *c*-CA has an active role in the regulation of plant development
533 remains an open and intriguing question; however, the fact that it was previously found in
534 small but physiologically relevant quantities in plants and that the effects on roots are
535 evolutionary conserved, only feeds the speculation on its importance as an endogenous
536 plant growth regulator (Yin et al., 2003; Wong et al., 2005). This function could be different
537 from lateral root development, a system that we only used to elucidate the molecular
538 mechanism of *c*-CA action.

539

540 MATERIAL AND METHODS

541 Plant material, transgenic lines, chemicals and growth conditions

542 The effect of *c/t*-CA on plant growth and development was studied in a diverse set of
543 plant species, comprising *Physcomitrella patens*, *Selaginella helvetica*, *Oryza sativa*,
544 *Nicotiana benthamiana*, *Brachypodium distachyon*, and *Arabidopsis thaliana*. *Arabidopsis*
545 *thaliana* ecotype Columbia (Col-0) was used, unless stated elsewhere. The used transgenic
546 lines were in the same ecotype: DII-VENUS, *DR5rev:GFP*, *DR5:LUC*, *pGATA23:GUS*,
547 *pGAZAT:GUS*, *pKNOLLE:KNOLLE-GFP*, *p35S:iaaL*, *slr*, *arf7 arf19* and *tir1 afb2 afb3*
548 (Romano et al., 1991; Lukowitz et al., 1996; Fukaki et al., 2002; Friml et al., 2003; Dharmasiri
549 et al., 2005; Gonzalez-Carranza et al., 2007; Okushima et al., 2007; De Rybel et al., 2010;
550 Moreno-Risueno et al., 2010; Brunoud et al., 2012). The transgenic line pCYCB1:GUS was
551 in the ecotype Landsberg Erecta (Ler) (Colon-Carmona et al., 1999). Seeds were vapor-
552 phase sterilized and grown on 0.5xMS-Medium. 0.5xMS medium (pH 5.7) contains per liter
553 1.5 g Murashige and Skoog basal salt mixture powder (Duchefa), 7.14 g sucrose, 0.36 g
554 MES monohydrate, 8 g plant tissue culture agar. The medium was supplemented with one of
555 the following compounds: naphthalene-1-acetic acid (NAA; Sigma Aldrich), 1-
556 naphthylphthalamic acid (NPA; Sigma Aldrich), *c*-CA (Shanghai Specbiochem CO., LTD) and
557 *t*-CA (Sigma Aldrich) from stock solutions in dimethyl sulfoxide (DMSO) (final 0.1% DMSO) to
558 the autoclaved medium prior to pouring the plates. After sowing, seeds were incubated at
559 4°C for at least 2 days whereupon plates were placed in a vertical orientation in the tissue
560 culture chamber room under a 16-hour-light/8-hour-dark photoperiod at 21°C, except for the
561 experiments done to reveal the pure *c*-CA and/or *t*-CA effect. Seedlings grown in darkness
562 received a short 4h red light-pulse to induce germination. Propidium-iodide (PI; Sigma
563 Aldrich) was used to counterstain the cell wall. The adventitious rooting assay was performed
564 by placing plates in darkness for seven days (after a short light-pulse with red light of 4
565 hours). Plates were then exposed to light for 5 days. The root bending assay was performed
566 on 5 days-old seedlings treated with different concentrations of *c/t*-CA. After 5 days plates
567 were rotated 90 degrees and root gravitropism was scored after 48 hours. Scans were made
568 and the quantification of the response was performed with ImageJ. Tobacco cells (*Nicotiana*
569 *tabacum* L., cv Bright Yellow-2) of the cell line BY-2 (Nagata et al., 1992) were cultivated
570 according to (Petrasek et al., 2006) and subcultured weekly. Bromophenol blue was used to
571 stain the cell wall of *Physcomitrella patens* leaves.

572

573 Description of plant phenotype

574 To quantify growth parameters and check for aberrant phenotypes, seeds were grown
575 on square plates placed in a vertical orientation in the growth chamber. Plates were scanned
576 using the Scanmaker 9800XL and root length was measured using the ImageJ software. For

577 each compound, the inhibitory concentration (IC_{50}) was calculated, plotting a dose-response
578 curve in SigmaPlot. The dose-response curve resulting in the highest R^2 -value (coefficient of
579 determination) was used. The number of plants used and the timing of the scanning depends
580 on the plant species and the treatment. The number of adventitious roots (above the root-
581 shoot junction) and number of emerged lateral roots were counted using a stereomicroscope
582 (CETI Binocular Zoom Stereo).

583

584 **Histochemical analysis and confocal microscopy**

585 Root cell walls were stained with 30 μ M PI for *pKNOLLE:KNOLLE-GFP* at the onset
586 of the experiment. The excitation energy of 488 nm was from an argon laser. The PI
587 fluorescence emission was collected between 550 and 650 nm, GFP/YFP between 500 and
588 550 nm. All images were captured with an inverted LSM 710 META confocal microscope
589 equipped with 20x-Air objectives (Carl Zeiss, Jena, Germany). GUS-assays were performed
590 and inspected using differential interference contrast optics as described earlier in Beeckman
591 and Engler (Beeckman and Engler, 1994)

592

593 **Time-lapse DII-VENUS**

594 For analysis of chemically treated roots, seven days-old DII-VENUS Arabidopsis
595 seedlings were transferred to 0.5xMS-media containing chemicals at the stated
596 concentration. At the onset of the time-lapse, 3 seedlings (biological repeats) were placed in
597 glass-bottomed dishes and covered with 0.5xMS-media containing NAA, NPA, *c*-CA or *t*-CA.
598 The time-lapse was started 5 min after the seedlings had been placed in contact with the
599 media and captured over 45 min (every 5 min) with an inverted LSM 710 META confocal
600 microscope equipped with 20x-Air objectives (Carl Zeiss, Jena, Germany). Images were
601 analyzed with the Fiji software using the total signal from Z-projection of defined region
602 (always the same area). Normalization was done by using the initial signal from the Z-
603 projection of a defined region as the baseline.

604

605 **Time-lapse DR5rev:GFP**

606 Seven days-old Arabidopsis seedlings were used to analyze the effect of *c*-CA, *t*-CA,
607 NPA and NAA on the expression of DR5rev:GFP in the region between two emerged lateral
608 roots. At the start of the time-lapse, seedlings were placed in glass-bottomed dishes and
609 covered with media containing NAA, *c*-CA or *t*-CA. The time-lapse was started 5 min after
610 the seedlings had been placed in contact with the media and captured over a period of 16h,
611 every hour with an inverted LSM 710 META confocal microscope (Carl Zeiss, Jena,
612 Germany) equipped with 20-Air objectives (Carl Zeiss, Jena, Germany). Images were
613 analyzed with the Volocity software. The accumulation projection spectrum was obtained by

614 projecting the GFP intensity on a virtual line crossing the middle of the primary root over the
615 imaged distance of the root. This way *DR5rev:GFP* expression can be imaged and quantified
616 in every cell type. Normalization was performed against the intensity to the highest obtained
617 signal at the earliest timepoint.

618

619 **Time-lapse *DR5:LUC***

620 The *DR5:LUC* images were taken by a Lumazone machine carrying a charge-coupled
621 device (CCD) camera (Princeton Instruments, Trenton, NJ, USA). The CCD camera that is
622 controlled by a WinView/32 software took movies of the *DR5:LUC* expression automatically
623 every 10 minutes (exposure time, 10 minutes) for 12 hours. Before imaging, plates
624 containing 0.5xMS-medium were sprayed with 1 mM D-luciferin solution (Duchefa
625 Biochemie). The picture series were saved as TIFF format for further analysis. The luciferase
626 signals were quantified by the measure of the analog-digital units (ADU) per pixel by means
627 of ImageJ. To visualize the spatiotemporal *DR5:LUC* signal changes during treatment with
628 the compound, a Kymograph (http://www.embl.de/eamnet/html/body_kymograph.html) was
629 generated with ImageJ.

630

631 **Heterologous expression of *C4H* and microsomes assay**

632 The *Saccharomyces cerevisiae* strain containing the Arabidopsis *C4H* was used (Van
633 de Wouwer et al., 2016). 100 μ L of recombinant yeast in glycerol was grown overnight at
634 30°C in 5 mL liquid DO medium (Clontech Laboratories Inc., Mountain View, CA, USA). The
635 yeast cells were pelleted (1 min at 4000 rpm), washed with 5 mL sterile MQ water, pelleted
636 again, and resuspended in another 5 mL water. The amount of inoculum was calculated to
637 reach an OD600 of 0.1 and subsequently, the yeast cultures were grown for 16h at 30°C with
638 shaking (200 rpm) in DO medium (Clontech Laboratories Inc., Mountain View, CA, USA)
639 containing galactose to induce transcription. Microsomes were prepared according to (Schalk
640 et al., 1998). The microsome assay was done with aliquots of 10 μ L microsome, by adding
641 20 mM sodium-phosphate-buffer (pH 7.4) (PBS), 10 μ L of the desired compound at final
642 concentrations of 10 μ M for *c*-CA and *t*-CA and equal amounts of DMSO as a control. To
643 start the reaction, 10 μ L of the 10 mM NADP⁺ PBS-solution was added to the Eppendorf,
644 briefly vortexed and immediately placed in the Eppendorf thermomixer at 28 °C for 20
645 minutes. The reaction was stopped by adding 150 μ L ice cold methanol. The pellet was
646 resuspended in 500 μ L 90% methanol and incubated in an Eppendorf thermomixer at 30°C
647 for 10 min while shaking at 1000 rpm. After centrifugation at 14 000 rpm for 5 min, the
648 supernatant was transferred to a new Eppendorf tube and lyophilized. The pellet was treated
649 with 100 μ L water and 100 μ L cyclohexane. After 10 min of centrifugation (14 000 rpm), 80
650 μ L of the aqueous phase was retained for UPLC-MS analysis. For reversed-phase LC, 10 μ L

651 of the aqueous phase was subjected to UPLC-MS on a Waters Acquity system (Waters
652 Corp., Milford, MA, USA) connected to a Thermo LTQ XL mass spectrometer (Thermo
653 Scientific, Waltham, MA, USA). Chromatographic gradient separation was carried out as
654 described in the next paragraph. The eluent was directed to the mass spectrometer via
655 electrospray ionization (ESI) in negative mode. MS source parameters were as follows:
656 capillary temperature, 300°C; capillary voltage, 24 V; source voltage, 3.5 V; source current,
657 100 A; sheath gas flow, 30; aux gas flow, 20; sweep gas flow, 5. The mass range was set
658 between 100 and 1000 Da. *c*-CA, *t*-CA and *p*-coumaric acid were characterized based on the
659 similarity of their masses and retention times with those of standards. Peak detection and
660 integration was done with Progenesis Q1 v2.1 (Nonlinear Dynamics, a Waters Company,
661 Newcastle, UK). Product/substrate ratios were calculated and p-values were calculated using
662 Unpaired Student T-Tests.

663

664 **Liquid chromatography-tandem mass spectrometry (LC-UV-Vis-MS) to** 665 **determine *c*- and *t*-CA photo-isomerization**

666 Exactly 2.5 mg of pure *t*-CA and *c*-CA was dissolved in 50.0 ml Milli-Q-H₂O/DMSO
667 (80/20). Solutions were subsequently incubated in the growth chamber and isomerization of
668 both isomers was followed over time by liquid chromatography-tandem mass spectrometry
669 (LC-MS/MS). For darkness, plates were covered with aluminum foil, to exclude light and
670 sampling was performed in darkness. Deep-red and far-red illumination was provided by the
671 GreenPower LED module, Philips.

672 For quantification of *t*-CA and *c*-CA a 15 µl aliquot was subjected to LC-MS analysis
673 performed on a Waters Acquity UPLC system equipped with a PDA detector (lambda range
674 from 190 to 500 nm) (Waters Corp., Milford, MA, USA) connected to a Synapt HDMS
675 quadrupole time-of-flight (Q-TOF) mass spectrometer (Waters MS Technologies,
676 Manchester, UK). Chromatographic separation was performed on an Acquity UPLC BEH
677 C18 column (2.1 mm × 150 mm, 1.7 µm; Waters Corp.) using a water-acetonitrile gradient
678 elution. Mobile phases were composed of (A) water containing 1% acetonitrile (ACN) and
679 0.1% formic acid and (B) ACN containing 1% water and 0.1% formic acid. The column
680 temperature was maintained at 40 °C, and the autosampler temperature was maintained at
681 10 °C. A flow rate of 350 µL/min was applied during the gradient elution, with initialization at
682 time 0 min 5% (B), 30 min 50% (B), and 33 min 100% (B). For UV-Vis detection, data was
683 recorded between 210 and 500 nm. The eluant was then directed to the mass spectrometer
684 equipped with an electrospray ionization source and lockspray interface for accurate mass
685 measurements. The MS source parameters were as follows: capillary voltage, 2.5 kV;
686 sampling cone, 37 V; extraction cone, 3.5 V; source temperature, 120°C; desolvation
687 temperature, 400°C; cone gas flow, 50 L h⁻¹; and desolvation gas flow, 550 L h⁻¹. The

688 collision energy for the trap and transfer cells was 6 and 4 V, respectively. For data
689 acquisition, the dynamic range enhancement mode was activated. Full-scan data were
690 recorded in negative centroid V-mode; the mass range between m/z 100 and 1000, with a
691 scan speed of 0.2 s scan^{-1} . Leucin-enkephalin ($250 \text{ pg } \mu\text{L}^{-1}$; solubilized in water: acetonitrile
692 1:1 [v/v] with 0.1% [v/v] formic acid) was used for lock mass calibration, with scanning every
693 10 s with a scan time of 0.5 s. All data was recorded with Masslynx software (version 4.1,
694 Waters). For the quantification of *t*-CA and *c*-CA, the UV-Vis chromatogram was extracted at
695 277nm, and peaks were integrated automatically (automatic noise measurement; mean
696 smoothing (window size: 3, number of smooths: 2)). Peak areas were used to calculate the
697 conversion of *t*-CA and *c*-CA.

698

699 **Auxin metabolite profiling**

700 Extraction and purification of auxin and its metabolites was done as described
701 previously with minor modifications (Novak et al., 2012). Frozen samples were homogenized
702 using a MixerMill (Retsch GmbH, Haan, Germany) and extracted in 1 mL 50 mM sodium
703 phosphate buffer (pH 7.0) containing antioxidant (1% sodium diethyldithiocarbamate) and a
704 cocktail of deuterium and $^{13}\text{C}_6$ -labeled internal standards of IAA and its metabolites. The pH
705 was adjusted to 2.7 with 1 M hydrochloric acid, and the extracts were purified on Oasis HLB
706 columns (30 mg, Waters Corp., Milford, USA), conditioned with 1 mL methanol, 1 mL water,
707 and 0.5 mL sodium phosphate buffer (pH 2.7). After sample application, the column was
708 washed with 2 mL 5% methanol and then eluted with 2 mL 80% methanol. Eluates were
709 evaporated to dryness and dissolved in 20 μL of mobile phase prior to mass analysis using a
710 1290 Infinity LC system and 6460 Triple Quad LC/MS system (Agilent Technologies, Santa
711 Clara, USA) (Novak et al., 2012).

712

713 **Auxin accumulation assays**

714 Assays were performed according to Petrášek *et al.* (Petrasek et al., 2003). Auxin
715 accumulation was measured in tobacco BY-2 cells (*Nicotiana tabacum* L. cv. Bright Yellow 2;
716 Nagata et al., 1992) 48 hours after subcultivation in 0.5 mL aliquots of cell suspension (target
717 working cell density was $7 \times 10^5 \text{ cells} \times \text{mL}^{-1}$, and it was determined precisely by counting in the
718 Fuchs-Rosenthal haemocytometer). Cultivation medium was removed by filtration on 20 μm
719 mesh nylon filters and cells were resuspended in uptake buffer (20 mM MES, 10 mM
720 sucrose, 0.5 mM CaSO_4 , pH adjusted to 5.7 with KOH) and equilibrated for 45 minutes on
721 the orbital shaker at 27 °C in darkness. Equilibrated cells were collected by filtration,
722 resuspended in fresh uptake buffer and incubated with continuous orbital shaking for another
723 90 minutes under the same conditions. Radiolabelled auxin ($[^3\text{H}]$ -naphthalene-1-acetic acid
724 ($[^3\text{H}]$ -NAA) or $[^3\text{H}]$ -2,4-dichlorophenoxyacetic acid ($[^3\text{H}]$ -2,4-D); specific (molar) radioactivity

725 20 Ci/mmol each; American Radiolabeled Chemicals, ARC Inc., St. Louis, MO, USA) was
726 added to the cell suspension to a final concentration of 2 nM. At certain time points, aliquots
727 of the cell suspension were sampled and accumulation of radiolabelled auxins was
728 terminated by rapid filtration under reduced pressure on cellulose filters (22 mm in diameter).
729 Cell cakes with filters were transferred into scintillation vials, extracted with ethanol (UV-
730 spectroscopy grade) for 30 minutes and radioactivity was determined by liquid scintillation
731 counting (Packard Tri-Carb 2900TR scintillation counter, Packard Instrument Co., Meriden,
732 CT, USA). Counting efficiency was determined by automatic external standardization and
733 counts were corrected for quenching automatically. For remaining surface radioactivity,
734 counts were corrected by subtracting counts of aliquots collected immediately after addition
735 of radiolabelled auxin. Inhibitors were added as required from stock solutions to an
736 appropriate final concentration and proper controls (solvent) were applied. Recorded
737 accumulation values were recalculated to 1 million cells.

738

739 **Rootward auxin transport assays**

740 Rootward auxin transport assays were performed as described previously (Geisler et
741 al., 2005). Briefly, 0.1 µL microdroplets containing 500 nM [³H]-IAA (American Radiolabelled
742 Chemicals) and 500 nM cold' IAA (Sigma Aldrich) were placed on the shoot apical meristem
743 of Arabidopsis seedlings and rootward auxin transport was measured by harvesting a 4 mm
744 segment centered on the root shoot transition zone, as well as the entire root, in 2 mm
745 segments (beginning with root zone-1 (RZ-1) just after the transition zone (TZ), and ending
746 with the main root tip). Treatments with MS-media and 10 µM *c*-CA were carried out by
747 saturating the filter paper matrix on which the roots were incubated during auxin transport
748 assays with MS media supplemented with either a water:methanol blank or *c*-CA.

749

750 **Auxin-binding and anti-auxin experiments using Surface Plasmon Resonance** 751 **(SPR) and docking**

752 Auxin receptor proteins AtTIR1 and AtAFB5 were expressed in insect cells (T. ni
753 High5) and purified as described previously (Villalobos et al., 2012; Lee et al., 2014). The
754 biotinylated degron peptide representing Aux/IAA7 was purchased from ThermoFisher
755 Scientific (Loughborough, UK) and immobilized on streptavidin-coated SPR chips (GE
756 Healthcare, Amersham, UK). SPR experiments were run as described previously (Villalobos
757 et al., 2012; Lee et al., 2014). Briefly, compounds were added to purified receptor proteins
758 from stock solutions in DMSO to give working concentrations which were 50 µM unless
759 stated otherwise (DMSO 0.1% final). Controls lacking auxin/compound and controls
760 containing IAA (50 µM) were run as references at the start and end of every set of
761 sensorgrams on every protein preparation. Compounds were run in three separate

762 experiments, with characteristic results shown. For anti-auxin runs, receptor proteins were
763 mixed with 5 μ M IAA plus compound at 50 μ M. An anti-auxin effect was then determined if
764 the compound competed with IAA, reducing the amplitude of TIR1/AFB5 binding on the
765 sensorgram. Docking was performed using the Vina docking algorithm (Morris et al., 2009;
766 Trott and Olson, 2010). With the TIR1 crystal structure (PDB code 2P1P) from (Tan et al.,
767 2007). In-silico modeling, molecular graphics and analyses were performed with the UCSF
768 Chimera package. Chimera is open source and developed by the Resource for
769 Biocomputing, Visualization, and Informatics at the University of California, San Francisco
770 (supported by NIGMS P41-GM103311) (Pettersen et al., 2004). Marvin was used for
771 drawing, displaying and characterizing chemical structures, substructures and reactions.
772 Calculator Plugins were used for structure property prediction and calculation
773 Marvin v15.10.12.0, 2015, ChemAxon (<http://www.chemaxon.com>).

774

775 **ACKNOWLEDGMENTS**

776

777 We would like to thank Ottoline Leyser (Sainsbury Laboratory, University of Cambridge,
778 Cambridge CB2 1LR) for providing us *p35S:iaaL* Arabidopsis seeds. We would like to thank Karel Spruyt
779 for imaging wherever needed, Toon Babylon for technical assistance, Wei Xua and Davy
780 Opdenacker for help with the *DR5:LUC* experiments and Tao Fang and Hans Motte for
781 providing us with the *Selaginella helvetica* plantlets.. We also appreciated the help of the VIB
782 Imaging Core facility, namely Amanda Gonçalves, who helped analyzing the imaging
783 experiments and Dominic Petrella for critical reading of the manuscript. Finally, we would like
784 to thank Wim Grunewald, Tom Beeckman, Steffen Vanneste, Bert De Rybel and Jürgen
785 Kleine-Vehn for scientific discussions.

786

787

788 **TABLES**

789

790 none

791

792

793 **FIGURE LEGENDS**

794

795 **Figure 1.** Effect of *c/t*-CA on growth and development of Arabidopsis.

796

797 (A) Root/rosette phenotype of representative seedlings 12 DAG, grown on 0.5xMS-medium
798 supplemented with *c/t*-CA ($n > 20$ for each concentration) (scale bar: 1 cm). (B) *c/t*-CA dose
799 response curve for primary root growth (Sigmoidal-logistic, 4 parameters) ($n > 20$). Error bars
800 represent standard deviations. (C) Lateral root density of seedlings 12 DAG, grown on
801 0.5xMS-medium supplemented with *c/t*-CA ($n > 15$). Error bars represent standard deviations
802 and asterisks were used to indicate statistically significant differences compared to the
803 corresponding mock-treated control sample as determined by Dunnett's test P-values: * $P <$
804 0.05 , ** $P < 0.001$, *** $P < 0.0001$. (D) Representative light microscopic images of a root
805 segment with lateral root primordia visualized by CYCB1:GUS expression in Arabidopsis 12
806 DAG of seedlings grown on 0.5xMS-medium supplemented with different concentrations of
807 *c/t*-CA ($n > 10$) (scale bar: 0.5 cm). (E) Number of adventitious roots of seedlings 12 DAG
808 grown on 0.5xMS-medium supplemented with *c/t*-CA. Plants were grown for 7 days in
809 darkness (after a short light-pulse of 4h with red-light to induce germination) and
810 subsequently transferred to light to stimulate adventitious rooting. Adventitious root numbers
811 are represented in grey-scale ($n > 20$). (F-G) Binocular microscopic images of a root segment
812 of the (F) primary root and (G) lateral root of seedlings 12 DAG, grown on 0.5xMS-medium

813 whether or not supplemented with 10 μM *c/t*-CA (n=10). (H) Histogram showing the *c/t*-CA-
814 induced disruption of the gravitropic response in the main root. Seeds were germinated on
815 0.5xMS-medium and 4 DAG seedlings were transferred to 0.5xMS-medium supplemented
816 with *c/t*-CA. Subsequently, seedlings growing on vertical plates were rotated 90 degrees and
817 each root was assigned to one of 12 30° sectors after 48h incubation (n>25).

818

819

820 **Figure 2.** Effect of *c*-CA on root architecture.

821

822 Dose response curves (Sigmoidal-logistic, 4 parameters) showing the effect of *c*-CA
823 (triangles) or *t*-CA (dots) on (A) hypocotyl and (B) root length of seedlings 12 DAG, grown in
824 darkness on 0.5xMS-medium supplemented with either *c*- or *t*-CA (n>20). Seed germination
825 was induced by a 4h red light-pulse. (C) Confocal images showing KNOLLE promoter activity
826 (green) of 10 DAG pKNOLLE:KNOLLE-GFP seedlings. (D-E) Light microscopic images of *c*-
827 CA induced GUS activity in 10 DAG pGAZAT:GUS and pGATA23:GUS seedlings. GUS
828 activity was monitored at the lateral roots (PGAZAT) or the zone basal to the main root tip
829 (GATA23). For the GATA23 driven GUS expression the main root tip is shown as inset. For
830 (C) and (D), seeds were germinated on 0.5xMS-medium and 7 DAG seedlings were
831 transferred to 0.5xMS-medium supplemented with 10 μM *c*-CA or *t*-CA (n=5) (scale bar: 15
832 μm). Growth conditions for (E) were as for (C) with the only exception that *c*-CA and *t*-CA
833 were used at 2.5 μM (n=5).

834

835

836 **Figure 3.** *c*-CA induces an auxin response in Arabidopsis.

837

838 (A) Kymograph of pDR5:LUC intensity along the primary root of Arabidopsis seedlings during
839 a 12h period. The kymograph represents on the vertical axis the primary root, with the root
840 tip present in the origin of the coordinate system, and the shoot/root junction at the end of
841 the vertical axis. The horizontal axis represents time. Seeds were germinated on 0.5xMS-
842 medium and 5 DAG seedlings were transferred to 0.5xMS-medium supplemented with 1-10
843 μM *c*-CA, 10 μM *t*-CA or 1 μM NAA. Imaging was started at the moment of transfer and data
844 was recorded every 10 minutes. Each kymograph represents one experiment. The
845 kymograph is representative for 8 biological repeats (seedlings). (B) Confocal time-lapse
846 imaging of pDR5rev:GFP intensity in the primary root between two young emerged lateral
847 roots. At the start of the time-lapse, seedlings were placed in glass-bottomed dishes and
848 covered with 0.5xMS-medium containing 1 μM NAA, 1-10 μM *c*-CA or 10 μM *t*-CA. The time-
849 lapse was started 5 minutes after the seedlings had been placed in contact with the media

850 and captured every 60 minutes over a 16h period. Cumulative spectra were obtained by
851 projecting the GFP intensity on a virtual line crossing the middle of the primary root.
852 Normalization was performed against the maximal intensity of the signal at the earliest time
853 point (n=1). Each spectrum is representative for 3 biological repeats (positions along the
854 primary root).

855

856

857 **Figure 4.** *c*-CA does not act as a typical auxin.

858

859 (A) Root phenotype of *arf7 arf19*, *slr* and *tir1 afb2 afb3* mutants 12 DAG, growing on 0.5xMS
860 medium supplemented with 10 μ M *c/t*-CA (n>25) (scale bar: 1 cm). (B) Surface Plasmon
861 Resonance sensorgrams showing the auxin-dependent interaction between TIR1 or AFB5
862 with IAA DII. Each sensorgram shows the binding with IAA (blue), an auxin-free injection
863 (red) plus the data for each test compound (green). For auxin activity assays (top)
864 compounds (50 μ M) were mixed with TIR1 or AFB5 prior to injection over DII peptide. For
865 anti-auxin assays (bottom), compounds (50 μ M) were mixed with TIR1 or AFB5 plus 5 μ M
866 IAA prior to injection. The degron sequence that was used: biot-AKAQVVGWPPVRNYRKN.

867

868

869 **Figure 5.** Effect of *c*-CA on polar auxin transport.

870

871 (A) Time-course of DII-VENUS fluorescence in the main root tip of DII-VENUS-YFP
872 seedlings. Plants were germinated on 0.5xMS-medium and subsequently transferred 5 DAG
873 to 0.5xMS-medium supplemented with 1 or 10 μ M *c*-CA, 10 μ M *t*-CA or 1 μ M 1-NAA (n=3).
874 (scale bar: 50 μ m). Fluorescence was quantified every 3 minutes over a 42 minute period.
875 During each experiment 3 root tips (representing one treatment) were simultaneously
876 imaged. Error bars represent standard deviations. (B) Effect of 10 μ M *c*-CA, *t*-CA or NPA on
877 the net accumulation of [3H]-NAA in 2-day old suspension-cultured tobacco BY-2 cells (20
878 minute uptake period). The arrows points to the time of application of the compound. Error
879 bars represent standard deviations (n=4). (C) Model explaining the *c*-CA mediated lateral
880 root proliferation. *c*-CA inhibits shootward auxin transport by inhibiting the redistribution of
881 auxin in the meristem. This is considered a direct consequence of the *c*-CA mediated
882 inhibition of auxin efflux. The phloem-mediated rootward auxin transport in the primary root is
883 not disturbed by *c*-CA, allowing a continuous supply of auxin from the shoot towards the root
884 tip. The block of a proper auxin redistribution in the meristem results in the accumulation of
885 auxin in the primary root, where it triggers lateral root proliferation. Top: auxin flow (blue
886 arrows) and its perturbation within the primary root of *c*-CA treated plants. Bottom: schematic

887 representation of auxin accumulation in the primary root of *c*-CA treated plants and the
888 consequent induction of lateral roots.

889

890

891 SUPPLEMENTAL FIGURES

892

893 **Figure S1.** The general phenylpropanoid pathway.

894 **Figure S2.** Effect of *c/t*-CA on growth and development of different plant species.

895 **Figure S3.** Photo-isomerization of *c*-CA and *t*-CA.

896 **Figure S4.** Conversion of *t*-CA by C4H in Arabidopsis.

897 **Figure S5.** Effect of *c*-CA on GATA23 expression.

898 **Figure S6.** Time dependent *DR5* driven *LUC* expression upon *c*-CA treatment.

899 **Figure S7.** Time dependent *DR5* driven *GFP* expression upon *c*-CA treatment.

900 **Figure S8.** Docking of *c*-CA and *t*-CA to the auxin binding pocket of TIR1.

901 **Figure S9.** Shift in IAA related metabolites upon treatment with 10 μ M *c*-CA and *t*-CA for 1h.

902 **Figure S10.** Shift in the IAA metabolome upon treatment with 10 μ M *c*-CA and *t*-CA for 6h.

903 **Figure S11.** The effect on IAA reduction on *c*-CA mediated developmental defects in
904 seedlings.

905 **Figure S12.** DII-VENUS response to *c*-CA.

906 **Figure S13.** DII-VENUS response to NPA.

907 **Figure S14.** The effect of combined treatment with *c*-CA and NPA on auxin accumulation.

908 **Figure S15.** The effect of combined treatment with *c*-CA and BUM on auxin accumulation.

909 **Figure S16.** The effect of *c*-CA on polar auxin transport.

910 **Figure S17.** Time dependent *DR5* driven *LUC* expression upon local application of
911 *c*-CA.

912 **Figure S18.** The effect of *c*-CA on long distance rootward auxin transport in Arabidopsis.

913

914

915

916

Parsed Citations

Åberg B (1961) Studies on plant growth regulator XVIII. Some β -substituted acrylic acids. Kungliga lantbrukshogskolans 27: 99-123

Pubmed: [Author and Title](#)

CrossRef: [Author and Title](#)

Google Scholar: [Author Only Title Only Author and Title](#)

Adamowski M, Friml J (2015) PIN-Dependent Auxin Transport: Action, Regulation, and Evolution. Plant Cell 27: 20-32

Pubmed: [Author and Title](#)

CrossRef: [Author and Title](#)

Google Scholar: [Author Only Title Only Author and Title](#)

Beeckman T, Engler G (1994) An easy technique for the clearing of histochemically stained plant tissue. Plant Molecular Biology Reporter 12: 37-42

Pubmed: [Author and Title](#)

CrossRef: [Author and Title](#)

Google Scholar: [Author Only Title Only Author and Title](#)

Benkova E, Michniewicz M, Sauer M, Teichmann T, Seifertova D, Jurgens G, Friml J (2003) Local, efflux-dependent auxin gradients as a common module for plant organ formation. Cell 115: 591-602

Pubmed: [Author and Title](#)

CrossRef: [Author and Title](#)

Google Scholar: [Author Only Title Only Author and Title](#)

Boerjan W, Ralph J, Baucher M (2003) Lignin biosynthesis. Annual Review of Plant Biology 54: 519-546

Pubmed: [Author and Title](#)

CrossRef: [Author and Title](#)

Google Scholar: [Author Only Title Only Author and Title](#)

Brown DE, Rashotte AM, Murphy AS, Normanly J, Tague BW, Peer WA, Taiz L, Muday GK (2001) Flavonoids act as negative regulators of auxin transport in vivo in Arabidopsis. Plant Physiology 126: 524-535

Pubmed: [Author and Title](#)

CrossRef: [Author and Title](#)

Google Scholar: [Author Only Title Only Author and Title](#)

Brunoud G, Wells DM, Oliva M, Larrieu A, Mirabet V, Burrow AH, Beeckman T, Kepinski S, Traas J, Bennett MJ, Vernoux T (2012) A novel sensor to map auxin response and distribution at high spatio-temporal resolution. Nature 482: 103-106

Pubmed: [Author and Title](#)

CrossRef: [Author and Title](#)

Google Scholar: [Author Only Title Only Author and Title](#)

Buer CS, Kordbacheh F, Truong TT, Hocart CH, Djordjevic MA (2013) Alteration of flavonoid accumulation patterns in transparent testa mutants disturbs auxin transport, gravity responses, and imparts long-term effects on root and shoot architecture. Planta 238: 171-189

Pubmed: [Author and Title](#)

CrossRef: [Author and Title](#)

Google Scholar: [Author Only Title Only Author and Title](#)

Colon-Carmona A, You R, Haimovitch-Gal T, Doerner P (1999) Spatio-temporal analysis of mitotic activity with a labile cyclin-GUS fusion protein. Plant Journal 20: 503-508

Pubmed: [Author and Title](#)

CrossRef: [Author and Title](#)

Google Scholar: [Author Only Title Only Author and Title](#)

De Rybel B, Vassileva V, Parizot B, Demeulenaere M, Grunewald W, Audenaert D, Van Campenhout J, Overvoorde P, Jansen L, Vanneste S, Moller B, Wilson M, Holman T, Van Isterdael G, Brunoud G, Vuylsteke M, Vernoux T, De Veylder L, Inze D, Weijers D, Bennett MJ, Beeckman T (2010) A Novel Aux/IAA28 Signaling Cascade Activates GATA23-Dependent Specification of Lateral Root Founder Cell Identity. Current Biology 20: 1697-1706

Pubmed: [Author and Title](#)

CrossRef: [Author and Title](#)

Google Scholar: [Author Only Title Only Author and Title](#)

Delbarre A, Muller P, Imhoff V, Guern J (1996) Comparison of mechanisms controlling uptake and accumulation of 2,4-dichlorophenoxy acetic acid, naphthalene-1-acetic acid, and indole-3-acetic acid in suspension-cultured tobacco cells. Planta 198: 532-541

Pubmed: [Author and Title](#)

CrossRef: [Author and Title](#)

Google Scholar: [Author Only Title Only Author and Title](#)

Dharmasiri N, Dharmasiri S, Weijers D, Lechner E, Yamada M, Hobbie L, Ehrismann JS, Jurgens G, Estelle M (2005) Plant development is regulated by a family of auxin receptor F box proteins. Developmental Cell 9: 109-119

Pubmed: [Author and Title](#)

CrossRef: [Author and Title](#)

Google Scholar: [Author Only Title Only Author and Title](#)

Ding ZJ, Galvan-Ampudia CS, Demarsy E, Langowski L, Kleine-Vehn J, Fan YW, Morita MT, Tasaka M, Fankhauser C, Offringa R, Friml J (2011) Light-mediated polarization of the PIN3 auxin transporter for the phototropic response in Arabidopsis. Nature Cell Biology 13: 447-453

Pubmed: [Author and Title](#)

CrossRef: [Author and Title](#)
Google Scholar: [Author Only Title Only Author and Title](#)

Friml J, Vieten A, Sauer M, Weijers D, Schwarz H, Hamann T, Offringa R, Jurgens G (2003) Efflux-dependent auxin gradients establish the apical-basal axis of Arabidopsis. Nature 426: 147-153

Pubmed: [Author and Title](#)
CrossRef: [Author and Title](#)
Google Scholar: [Author Only Title Only Author and Title](#)

Fukaki H, Tameda S, Masuda H, Tasaka M (2002) Lateral root formation is blocked by a gain-of-function mutation in the SOLITARY-ROOT/IAA14 gene of Arabidopsis. Plant Journal 29: 153-168

Pubmed: [Author and Title](#)
CrossRef: [Author and Title](#)
Google Scholar: [Author Only Title Only Author and Title](#)

Gonzalez-Carranza ZH, Elliott KA, Roberts JA (2007) Expression of polygalacturonases and evidence to support their role during cell separation processes in Arabidopsis thaliana. J Exp Bot 58: 3719-3730

Pubmed: [Author and Title](#)
CrossRef: [Author and Title](#)
Google Scholar: [Author Only Title Only Author and Title](#)

Haagen-Smit SAJW, F.W. (1935) A physiological analysis of the growth substance. Proceedings, Koninklijke Akademie van Wetenschappen te Amsterdam 38: 852-857

Pubmed: [Author and Title](#)
CrossRef: [Author and Title](#)
Google Scholar: [Author Only Title Only Author and Title](#)

Hitchcock AE (1935) Indole-3-n-propionic acid as a growth hormone and quantitative measurement of plant response. Contributions from Boyce Thompson Institute 7: 87-95

Pubmed: [Author and Title](#)
CrossRef: [Author and Title](#)
Google Scholar: [Author Only Title Only Author and Title](#)

Hoyerova K, Hosek P, Kubes M, Lankova M, Kohoutova M, Dobrev PI, Jirina M, Petrasek J, Zazimalova E (2011) Auxin transport on cellular level by means of mathematical-modelling-motivated research. Febs Journal 278: 314-314

Pubmed: [Author and Title](#)
CrossRef: [Author and Title](#)
Google Scholar: [Author Only Title Only Author and Title](#)

Kim JY, Henrichs S, Bailly A, Vincenzetti V, Sovero V, Mancuso S, Pollmann S, Kim D, Geisler M, Nam HG (2010) Identification of an ABCB/P-glycoprotein-specific Inhibitor of Auxin Transport by Chemical Genomics. Journal of Biological Chemistry 285: 23307-23315

Pubmed: [Author and Title](#)
CrossRef: [Author and Title](#)
Google Scholar: [Author Only Title Only Author and Title](#)

Koepfli JB, Thimann KB, Went FW (1938) Plant hormones: structure and physiological activity. Journal of Biological Chemistry 122: 763-780

Pubmed: [Author and Title](#)
CrossRef: [Author and Title](#)
Google Scholar: [Author Only Title Only Author and Title](#)

Kumpf RP, Shi CL, Larrieu A, Sto IM, Butenko MA, Peret B, Riiser ES, Bennett MJ, Aalen RB (2013) Floral organ abscission peptide IDA and its HAE/HSL2 receptors control cell separation during lateral root emergence. Proc Natl Acad Sci U S A 110: 5235-5240

Pubmed: [Author and Title](#)
CrossRef: [Author and Title](#)
Google Scholar: [Author Only Title Only Author and Title](#)

Lee S, Sundaram S, Armitage L, Evans JP, Hawkes T, Kepinski S, Ferro N, Napier RM (2014) Defining Binding Efficiency and Specificity of Auxins for SCFTIR1/AFB-Aux/IAA Co-receptor Complex Formation. Acs Chemical Biology 9: 673-682

Pubmed: [Author and Title](#)
CrossRef: [Author and Title](#)
Google Scholar: [Author Only Title Only Author and Title](#)

Letham DS (1978) Natural-occurring plant growth regulations other than the principal hormones of higher plants. Phytohormones and Related Compounds - A Comprehensive Treatise 38: 85-92

Pubmed: [Author and Title](#)
CrossRef: [Author and Title](#)
Google Scholar: [Author Only Title Only Author and Title](#)

Liu CM, Xu ZH, Chua NH (1993) Auxin Polar Transport Is Essential for the Establishment of Bilateral Symmetry during Early Plant Embryogenesis. Plant Cell 5: 621-630

Pubmed: [Author and Title](#)
CrossRef: [Author and Title](#)
Google Scholar: [Author Only Title Only Author and Title](#)

Lukowitz W, Mayer U, Jurgens G (1996) Cytokinesis in the Arabidopsis embryo involves the syntaxin-related KNOLLE gene product. Cell 84: 61-71

Pubmed: [Author and Title](#)
CrossRef: [Author and Title](#)
Google Scholar: [Author Only Title Only Author and Title](#)

Moreno-Risueno MA, Van Norman JM, Moreno A, Zhang JY, Ahnert SE, Benfey PN (2010) Oscillating Gene Expression Determines Competence for Periodic Arabidopsis Root Branching. *Science* 329: 1306-1311

Pubmed: [Author and Title](#)

CrossRef: [Author and Title](#)

Google Scholar: [Author Only](#) [Title Only](#) [Author and Title](#)

Morris GM, Huey R, Lindstrom W, Sanner MF, Belew RK, Goodsell DS, Olson AJ (2009) AutoDock4 and AutoDockTools4: Automated Docking with Selective Receptor Flexibility. *Journal of Computational Chemistry* 30: 2785-2791

Pubmed: [Author and Title](#)

CrossRef: [Author and Title](#)

Google Scholar: [Author Only](#) [Title Only](#) [Author and Title](#)

Nagata T, Nemoto Y, Hasezawa S (1992) Tobacco by-2 Cell-Line as the HeLa-Cell in the Cell Biology of Higher-Plants. *International Review of Cytology-a Survey of Cell Biology* 132: 1-30

Pubmed: [Author and Title](#)

CrossRef: [Author and Title](#)

Google Scholar: [Author Only](#) [Title Only](#) [Author and Title](#)

Novak O, Henykova E, Sairanen I, Kowalczyk M, Pospisil T, Ljung K (2012) Tissue-specific profiling of the Arabidopsis thaliana auxin metabolome. *Plant Journal* 72: 523-536

Pubmed: [Author and Title](#)

CrossRef: [Author and Title](#)

Google Scholar: [Author Only](#) [Title Only](#) [Author and Title](#)

Okushima Y, Fukaki H, Onoda M, Theologis A, Tasaka M (2007) ARF7 and ARF19 regulate lateral root formation via direct activation of LBD/ASL genes in Arabidopsis. *Plant Cell* 19: 118-130

Pubmed: [Author and Title](#)

CrossRef: [Author and Title](#)

Google Scholar: [Author Only](#) [Title Only](#) [Author and Title](#)

Peret B, De Rybel B, Casimiro I, Benkova E, Swarup R, Laplaze L, Beeckman T, Bennett MJ (2009) Arabidopsis lateral root development: an emerging story. *Trends Plant Sci* 14: 399-408

Pubmed: [Author and Title](#)

CrossRef: [Author and Title](#)

Google Scholar: [Author Only](#) [Title Only](#) [Author and Title](#)

Petrasek J, Cerna A, Schwarzerova K, Eickner M, Morris DA, Zazimalova E (2003) Do phytohormones inhibit auxin efflux by impairing vesicle traffic? *Plant Physiology* 131: 254-263

Pubmed: [Author and Title](#)

CrossRef: [Author and Title](#)

Google Scholar: [Author Only](#) [Title Only](#) [Author and Title](#)

Petrasek J, Mravec J, Bouchard R, Blakeslee JJ, Abas M, Seifertova D, Wisniewska J, Tadele Z, Kubes M, Covanova M, Dhonukshe P, Skupa P, Benkova E, Perry L, Krecek P, Lee OR, Fink GR, Geisler M, Murphy AS, Luschnig C, Zazimalova E, Friml J (2006) PIN proteins perform a rate-limiting function in cellular auxin efflux. *Science* 312: 914-918

Pubmed: [Author and Title](#)

CrossRef: [Author and Title](#)

Google Scholar: [Author Only](#) [Title Only](#) [Author and Title](#)

Pettersen EF, Goddard TD, Huang CC, Couch GS, Greenblatt DM, Meng EC, Ferrin TE (2004) UCSF chimera - A visualization system for exploratory research and analysis. *Journal of Computational Chemistry* 25: 1605-1612

Pubmed: [Author and Title](#)

CrossRef: [Author and Title](#)

Google Scholar: [Author Only](#) [Title Only](#) [Author and Title](#)

Romano CP, Hein MB, Klee HJ (1991) Inactivation of Auxin in Tobacco Transformed with the Indoleacetic-Acid Lysine Synthetase Gene of Pseudomonas-Savastanoi. *Genes & Development* 5: 438-446

Pubmed: [Author and Title](#)

CrossRef: [Author and Title](#)

Google Scholar: [Author Only](#) [Title Only](#) [Author and Title](#)

Santelia D, Henrichs S, Vincenzetti V, Sauer M, Bigler L, Klein M, Bailly A, Lee Y, Friml J, Geisler M, Martinoia E (2008) Flavonoids Redirect PIN-mediated Polar Auxin Fluxes during Root Gravitropic Responses. *Journal of Biological Chemistry* 283: 31218-31226

Pubmed: [Author and Title](#)

CrossRef: [Author and Title](#)

Google Scholar: [Author Only](#) [Title Only](#) [Author and Title](#)

Schalk M, Cabello-Hurtado F, Pierrel MA, Atanossova R, Saindrenan P, Werck-Reichhart D (1998) Piperonylic acid, a selective, mechanism-based inactivator of the trans-cinnamate 4-hydroxylase: A new tool to control the flux of metabolites in the phenylpropanoid pathway. *Plant Physiology* 118: 209-218

Pubmed: [Author and Title](#)

CrossRef: [Author and Title](#)

Google Scholar: [Author Only](#) [Title Only](#) [Author and Title](#)

Trott O, Olson AJ (2010) Software News and Update AutoDock Vina: Improving the Speed and Accuracy of Docking with a New Scoring Function, Efficient Optimization, and Multithreading. *Journal of Computational Chemistry* 31: 455-461

Pubmed: [Author and Title](#)

CrossRef: [Author and Title](#)

Google Scholar: [Author Only](#) [Title Only](#) [Author and Title](#)

Van Overbeek J, Blondeau R, Horne V (1951) Trans-cinnamic acid as an anti-auxin. American Journal of Botany 38: 589-595

Pubmed: [Author and Title](#)

CrossRef: [Author and Title](#)

Google Scholar: [Author Only](#) [Title Only](#) [Author and Title](#)

Vanneste S, Friml J (2009) Auxin: A Trigger for Change in Plant Development. Cell 136: 1005-1016

Pubmed: [Author and Title](#)

CrossRef: [Author and Title](#)

Google Scholar: [Author Only](#) [Title Only](#) [Author and Title](#)

Villalobos LIAC, Lee S, De Oliveira C, Ivetac A, Brandt W, Armitage L, Sheard LB, Tan X, Parry G, Mao HB, Zheng N, Napier R, Kepinski S, Estelle M (2012) A combinatorial TIR1/AFB-Aux/IAA co-receptor system for differential sensing of auxin. Nature Chemical Biology 8: 477-485

Pubmed: [Author and Title](#)

CrossRef: [Author and Title](#)

Google Scholar: [Author Only](#) [Title Only](#) [Author and Title](#)

Vogt T (2010) Phenylpropanoid Biosynthesis. Molecular Plant 3: 2-20

Pubmed: [Author and Title](#)

CrossRef: [Author and Title](#)

Google Scholar: [Author Only](#) [Title Only](#) [Author and Title](#)

Went FW (1939) Analysis and integration of various auxin effects. I and II. Proceedings, Koninklijke Akademie van Wetenschappen te Amsterdam XLII: 731-739

Pubmed: [Author and Title](#)

CrossRef: [Author and Title](#)

Google Scholar: [Author Only](#) [Title Only](#) [Author and Title](#)

Wong WS, Guo D, Wang XL, Yin ZQ, Xia B, Li N (2005) Study of cis-cinnamic acid in Arabidopsis thaliana. Plant Physiology and Biochemistry 43: 929-937

Pubmed: [Author and Title](#)

CrossRef: [Author and Title](#)

Google Scholar: [Author Only](#) [Title Only](#) [Author and Title](#)

Yang XX, Choi HW, Yang SF, Li N (1999) A UV-light activated cinnamic acid isomer regulates plant growth and gravitropism via an ethylene receptor-independent pathway. Aust J Plant Physiol 26: 325-335

Pubmed: [Author and Title](#)

CrossRef: [Author and Title](#)

Google Scholar: [Author Only](#) [Title Only](#) [Author and Title](#)

Yin RH, Han K, Heller W, Albert A, Dobrev PI, Zazimalova E, Schaffner AR (2014) Kaempferol 3-O-rhamnoside-7-O-rhamnoside is an endogenous flavonol inhibitor of polar auxin transport in Arabidopsis shoots. New Phytologist 201: 466-475

Pubmed: [Author and Title](#)

CrossRef: [Author and Title](#)

Google Scholar: [Author Only](#) [Title Only](#) [Author and Title](#)

Yin ZQ, Wong WS, Ye WC, Li N (2003) Biologically active cis-cinnamic acid occurs naturally in Brassica parachinensis. Chinese Science Bulletin 48: 555-558

Pubmed: [Author and Title](#)

CrossRef: [Author and Title](#)

Google Scholar: [Author Only](#) [Title Only](#) [Author and Title](#)